JOURNAL OF GEOPHYSICAL RESEARCH, VOL. 114, B10405, doi:10.1029/2009JB006416, 2009

Absolute plate motions constrained by shear wave splitting orientations with implications for hot spot motions and mantle flow

Corné Kreemer[1]

Received 27 February 2009; revised 11 June 2009; accepted 14 July 2009; published 22 October 2009.

[1] Here, I present a new absolute plate motion model of the Earth's surface, determined from the alignment of present-day surface motions with 474 published shear wave (i.e., SKS) splitting orientations. When limited to oceanic islands and cratons, splitting orientations are assumed to reflect anisotropy in the asthenosphere caused by the differential motion between lithosphere and mesosphere. The best fit model predicts a 0.2065°/Ma counterclockwise net rotation of the lithosphere as a whole, which revolves around a pole at 57.6°S and 63.2°E. This net rotation is particularly well constrained by data on cratons and/or in the Indo-Atlantic region. The average data misfit is 19° and 24° for oceanic and cratonic areas, respectively, but the normalized root-mean-square misfits are about equal at 5.4 and 5.2. Predicted plate motions are very consistent with recent hot spot track azimuths (<8° on many plates), except for the slowest moving plates (Antarctica, Africa, and Eurasia). The difference in hot spot propagation vectors and plate velocities describes the motion of hot spots (i.e., their underlying plumes). For most hot spots that move significantly, the motions are considerably smaller than and antiparallel to the absolute plate velocity. Only when the origin depth of the plume is considered can the hot spot motions be explained in terms of mantle flow. The results are largely consistent with independent evidence of subasthenospheric mantle flow and asthenospheric return flow near spreading ridges. The results suggest that, at least where hot spots are, the lithosphere is decoupled from the mesosphere, including in western North America.

Citation: Kreemer, C. (2009), Absolute plate motions constrained by shear wave splitting orientations with implications for hot spot motions and mantle flow, *J. Geophys. Res.*, *114*, B10405, doi:10.1029/2009JB006416.

1. Introduction

[2] The term "absolute plate motion" (APM) is generally used to indicate the motion of Earth's surface or lithosphere relative to the deep (and assumed stable) mantle. APM models, which describe motions for most or all of the Earth's surface, are widely used in modeling and understanding mantle flow and anisotropy, plate driving forces, and the dynamics of subduction zones, among others. Although APM estimates are key to linking deep Earth processes with tectonics and surface motions, APM is still poorly known and current models vary significantly among each other. Consequently, our understanding of a given geodynamic process depends on the choice of APM model [e.g., *Kubo and Hiramatsu*, 1998; *Barruol and Hoffmann*, 1999; *Simons and van der Hilst*, 2003; *Becker et al.*, 2007; *Funiciello et al.*, 2008]. As a result of the diversity in APM models, recent studies have started to "rank" published APM models by their ability to explain a set of observations or a chosen geodynamical model [e.g., *Lallemand et al.*, 2008; *Schellart et al.*, 2008; *Long and Silver*, 2009].

[3] There are generally five concepts that underpin APM models: (1) hot spot plumes have a lower mantle source [*Morgan*, 1971]; (2) the lithosphere does not rotate as a whole with respect to the lower mantle [*Lliboutry*, 1974; *Solomon and Sleep*, 1974]; (3) some plates, such as Africa or Antarctica, are stationary relative to the lower mantle [*Le Pichon*, 1968; *Burke and Wilson*, 1972; *Hamilton*, 2003]; (4) the lateral migration of spreading ridges and/or trenches should be minimized globally [*Kaula*, 1975; *Schellart et al.*, 2008]; and (5) motion should be perpendicular to trenches and ridges [*Gordon et al.*, 1978].

[4] The idea that there is no net rotation (NNR) of the entire lithosphere can be (and has been) discounted, because basal shear beneath stiff continental keels causes a net rotation [e.g., *O'Connell et al.*, 1991; *Ricard et al.*, 1991; *Zhong*, 2001; *Becker*, 2006]. A certain level of net rotation can also be deduced from recent mantle flow studies that aimed to match predicted finite strain orientations with seismic anisotropy orientations in the mantle [e.g., *Behn et al.*, 2004; *Becker*, 2006; *Conrad et al.*, 2007]. The net rotation is likely to be much smaller (~50%) than that implied by the recent hot spot model HS3-NUVEL1A of *Gripp and Gordon* [2002]. However, it is unclear whether this discrepancy implies an incomplete understanding of mantle dynamics, uncertainties in hot spot models, or both [*Becker*, 2008].

[1]Nevada Bureau of Mines and Geology and Seismological Laboratory, University of Nevada, Reno, Reno, Nevada, USA.

0148-0227/09/2009JB006416$09.00

[5] The most widely used APM models are those using hot spot track data [e.g., *Minster and Jordan*, 1978; *Gordon and Jurdy*, 1986; *Gripp and Gordon*, 2002]. Hot-spot-based APM models typically assume that plumes are fixed in the lower mantle, and that hot spot tracks record lithospheric motion over the plume [*Wilson*, 1963; *Morgan*, 1971]. However, not all plumes originate in the lower mantle [e.g., *Zhao*, 2001; *Courtillot et al.*, 2003; *Montelli et al.*, 2006; *Boschi et al.*, 2007] or are fixed with respect to each other [e.g., *Molnar and Stock*, 1987; *Tarduno and Gee*, 1995; *DiVenere and Kent*, 1999; *Koppers et al.*, 2001; *O'Neill et al.*, 2003]. To accommodate the latter observation, newer hot-spot-derived APM models consider only hot spot data in the Pacific domain (e.g., HS3-NUVEL1A) or the Indo-Atlantic domain [e.g., *Müller et al.*, 1993]. More recently, some APM models have allowed the hot spot plumes to move as consistent with mantle flow predictions [*Steinberger et al.*, 2004; *O'Neill et al.*, 2005; *Torsvik et al.*, 2008]. Yet another set of studies have considered only hot spot trends, not velocities [*Wang and Wang*, 2001; *Morgan and Phipps Morgan*, 2007]. Those latter studies found APM rates that were considerably slower than, e.g., HS3-NUVEL1A and may suggest (1) a component of lower-mantle counterflow and (2) a level of net rotation consistent with that found in the aforementioned geodynamic studies. However, the studies by *Morgan and Phipps Morgan* [2007] and *Wang and Wang* [2001] suffer from limited reliable hot spot tracks, with most located in the fast-moving Pacific basin. Instead, the strongest constraint on the lithosphere's net rotation would come from orientation data in the slow-moving Atlantic-Indian Ocean area. Data in the Pacific, on the other hand, is aligned to the net rotation direction for any rotation rate.

[6] In this study, I present a new present-day APM model that is not based on hot spot data, but on the orientations of shear wave splitting observations from oceanic islands and cratons. The underlying assumption is that those splitting measurements predominantly indicate asthenospheric anisotropy, which in turn reflects the motion between the lithosphere and subasthenospheric mantle (or mesosphere). I solve for a rigid body rotation that represents the net rotation of global lithosphere, and minimizes the global misfit between anisotropy orientations and velocity azimuths of present-day relative plate motions. A full APM model can then be derived by adding the net rotation to the known surface motions in a NNR reference frame. Because the APM model is hot spot independent, I use hot spot track data as "piercing points" to infer the underlying plume motion relative to the mesosphere. Using independent evidence of plume depth, I interpret hot spot motions in terms of the first-order characteristics of the underlying mantle flow field.

[7] In contrast to recent studies that compared mantle flow models with anisotropy orientations and some level of lithospheric net rotation [*Becker*, 2006, 2008], this study is purely kinematic. My primary assumption relies on a first-order relationship between APM and asthenospheric anisotropy. This study is conducted on a global scale to avoid the effects of regional density-driven mantle flow on mantle anisotropy [e.g., *Behn et al.*, 2004]. I use a large number of widely distributed anisotropy data, so that any second-order regional deviations are minimized.

2. Seismic Anisotropy and APM

[8] To estimate an APM model using shear wave (i.e., mainly SKS) splitting observations, it is assumed that (1) SKS anisotropy originates in the asthenosphere and aligns with APM at a sufficient number of global locations to allow for a robust inversion and (2) finite mantle strain directions align equally well to present-day plate motions as to plate motions integrated over time. The appropriateness of these assumptions is discussed below.

2.1. Oceanic Mantle

[9] The first assumption made above is generally valid underneath oceanic lithosphere. There, anisotropy is predicted (as lattice preferred orientation (LPO)) [e.g., *Zhang and Karato*, 1995; *Tommasi et al.*, 1996; *Tommasi*, 1998; *Podolefsky et al.*, 2004] and observed [e.g., *Montagner and Tanimoto*, 1991; *Lévêque et al.*, 1998; *Maggi et al.*, 2006] to originate between 100 and 300 km depth in the asthenosphere, in response to simple shear induced by the differential motion between the lithosphere and mesosphere. Most studies of oceanic SKS splitting find that splitting orientations φ_{SKS} generally align with φ_{APM} predicted by existing APM models [e.g., *Russo and Okal*, 1998; *Wolfe and Silver*, 1998; *Klosko et al.*, 2001; *Fontaine et al.*, 2007]. Some of the seismic polarization observed at island stations may originate within the oceanic lithosphere and align with paleo-spreading directions [*Blackman and Kendall*, 2002; *Becker et al.*, 2003; *Fontaine et al.*, 2007]. However, such lithospheric anisotropy contributes far less to splitting observations than anisotropy in the asthenosphere [*Behn et al.*, 2004]. Close to spreading ridges, shear wave polarization may reflect small-scale convection or spreading-induced flow [e.g., *Wolfe and Solomon*, 1998; *Blackman and Kendall*, 2002; *Becker et al.*, 2003; *Harmon et al.*, 2004]. However, this flow is typically parallel to APM and will not invalidate my assumption of φ_{SKS} being aligned to φ_{APM}. In any case, no data within 50–100 km from a spreading ridge is included in this study.

2.2. Continental Mantle

[10] The assumptions that observed anisotropy originates within the asthenosphere and that φ_{SKS} aligns with φ_{APM} are only partly true for measurements made on continents. In many continental areas, φ_{SKS} observations deviate significantly from φ_{APM}, and vary rapidly between stations due to the presence of lithospheric anisotropy. Lithospheric anisotropy can be attributed to active tectonics, acquired lithospheric structure, and/or entrained flow around continental keels [e.g., *Silver*, 1996; *Fouch and Rondenay*, 2006]. Moreover, even if the lithosphere is isotropic, mantle flow fields beneath tectonically active areas are rarely aligned with φ_{APM} due to, for example, the complex flow fields around subduction slabs or the boundary-parallel flow in transform plate boundaries [e.g., *Savage*, 1999; *Park and Levin*, 2002; *Long and Silver*, 2008].

[11] A recent global study compared published φ_{SKS} values with predicted LPO orientations from mantle flow calculations and plate motions. *Conrad et al.* [2007] con-

cluded that asthenospheric anisotropy beneath stable continents contributes to some level to observed splitting. Those results are consistent with findings that anisotropy below cratons is aligned to φ_{APM} (at least for North America and Australia) when anisotropy in and below the lithosphere is separated [e.g., *Levin et al.*, 2000; *Simons and van der Hilst*, 2003; *Marone and Romanowicz*, 2007; *Deschamps et al.*, 2008; *Yuan et al.*, 2008]. *Debayle et al.* [2005] found asthenospheric (APM controlled) anisotropy underneath Australia, but nowhere else. It has been argued [*Gung et al.*, 2003; *Marone and Romanowicz*, 2007] that *Debayle et al.* [2005] did not find similar results for other continents than Australia because of a possibly reduced sensitivity of the surface wave approach.

[12] I limit continental data in my model to cratons/shields to minimize lithospheric anisotropy on φ_{SKS} measurements, and to optimize the likelihood that φ_{SKS} on continents reflects asthenospheric anisotropy. For some cratons (e.g., Canadian shield, east-central South America, India), φ_{SKS} and φ_{APM} appear to generally align, and APM appears thus to control observed anisotropy [e.g., *Vinnik et al.*, 1992; *Kay et al.*, 1999; *Bank et al.*, 2000; *Bokelmann*, 2002a; *Assumpção et al.*, 2006; *Frederiksen et al.*, 2006; *Kumar and Singh*, 2008]. For other cratons (e.g., Australia, Greenland, Arabia) such consistency was not observed [e.g., *Heintz and Kennett*, 2005; *Hansen et al.*, 2006; *Ucisik et al.*, 2008]. Some of the discrepancy may be explained by a component of density-driven flow in the asthenosphere (e.g., underneath Arabia [*Hansen et al.*, 2006]; see section 2.3), a modification of the asthenospheric flow field around keels [e.g., *Fouch et al.*, 2000; *Eaton et al.*, 2004; *Heintz and Kennett*, 2005; *Gao et al.*, 2008], and a significant lithospheric contribution (e.g., Australia [e.g., *Simons and van der Hilst*, 2003; *Heintz and Kennett*, 2005] and east Antarctica [*Reading and Heintz*, 2008]). Some other reported discrepancies between φ_{SKS} and φ_{APM} may have resulted from the large range of published φ_{APM} [e.g., *Heintz et al.*, 2003; *Evans et al.*, 2006] or from the use of an inappropriate APM model (e.g., NNR in Antarctica [*Reading and Heintz*, 2008], or HS2-NUVEL1A in Africa [*Barruol and Ben Ismail*, 2001]).

2.3. Density-Driven Mantle Flow

[13] When asthenospheric anisotropy is assumed to align with φ_{APM}, the APM model velocities $\vec{v}_{APM}$ are implicitly relative to the top of the mesosphere. The mesosphere is however not completely fixed, and may be affected by large-scale flow induced by regional density variations [e.g., *Forte and Mitrovica*, 2001; *Becker et al.*, 2003; *Gaboret et al.*, 2003; *Behn et al.*, 2004]. In most cases, mesospheric flow is small compared to $\vec{v}_{APM}$, and is generally antiparallel to $\vec{v}_{APM}$ (i.e., away from subduction zone downwellings and toward upwellings) [e.g., *Forte and Mitrovica*, 2001]. It should be noted here that mesospheric counterflow is expected in the absence of any density variations, and may be caused by a plate moving on top of a very weak asthenosphere [e.g., *Hager and O'Connell*, 1979]. Either way, in most cases, any counterflow in the mesosphere would not significantly affect splitting orientations.

[14] Density-driven mantle flow also affects anisotropy orientations in the asthenosphere. In most cases, particularly for fast-moving plates, expected and observed anisotropy orientations are roughly parallel when density-driven flow is considered (with or without an APM boundary condition at the surface) [e.g., *Becker et al.*, 2003; *Gaboret et al.*, 2003; *Conrad et al.*, 2007]. However, in cases of significant density-driven flow underneath slow-moving plates, incorrect $\vec{v}_{APM}$ could be inferred if φ_{SKS} is assumed to mainly reflect φ_{APM} (even in the case the mesosphere is fixed). For instance, *Behn et al.* [2004] showed that φ_{SKS} observations around Africa are best explained by LPO orientations predicted by a model that includes plate motions and density-driven flow. However, the effect of density-driven flow on anisotropy orientations is nonsystematic on a global scale, and a first-order relationship between φ_{APM} and φ_{SKS} can be assumed.

2.4. Constancy of Plate Motions

[15] The second assumption made at the beginning of the section, that present-day plate motions align with past plate motions and thus with φ_{SKS}, is to first order appropriate. Plate velocities have been nearly constant over at least the last 3 Ma [e.g., *Sella et al.*, 2002; *Kreemer et al.*, 2003] and possibly up to 40 Ma for the major plates (particularly when hot spots are not considered to be fixed) [e.g., *Wang and Liu*, 2006]. Given the rate of plate motions, these times are long enough to align LPO in the asthenosphere to φ_{APM} [e.g., *Zhang and Karato*, 1995; *Tommasi et al.*, 1996; *Kaminski and Ribe*, 2002]. Some of the most significant recent plate motion changes are, for example, the decelerations of India between 20 and 11 Ma [e.g., *Merkouriev and DeMets*, 2006] and Nazca between 15 Ma and present [e.g., *Somoza*, 1998; *Kendrick et al.*, 2003]. However, these decelerations generally do not change the direction of plate motion, and do therefore not affect φ_{APM}.

3. Approach

[16] I compiled a data set of φ_{SKS} estimates from published shear wave splitting measurements. To avoid including φ_{SKS} measurements affected by active tectonics, I exclude any data obtained within the (present-day) plate boundary zones as defined by the Global Strain Rate Map (GSRM) [*Kreemer et al.*, 2003]. To further avoid including measurements that reflect lithospheric structure, I limit continental data to those obtained above cratons. Some lithospheric anisotropy could still exist, however, and may be more significant than anisotropy in the underlying asthenosphere (because subcratonic asthenosphere may be relatively thin and continents typically move slowly). I will, however, describe below how the inclusion of cratonic φ_{SKS} observations is justified.

[17] I restrict data to the cratonic parts of continents by using craton outlines of *Artemieva and Mooney* [2002], supplemented with an Antarctic shield outline based on the tomographic results of *Ritzwoller et al.* [2001]. In general, φ_{SKS} is taken from studies assuming single-layer anisotropy. If only two-layer results are given, the φ_{SKS} that corresponds to the lower layer (presumably the asthenosphere) is used. The 474 φ_{SKS} measurements (at 413 locations) used in this study are summarized in the auxiliary material and shown in Figure 1.[1]

[1] Auxiliary materials are available in the HTML. doi:10.1029/2009JB006416.

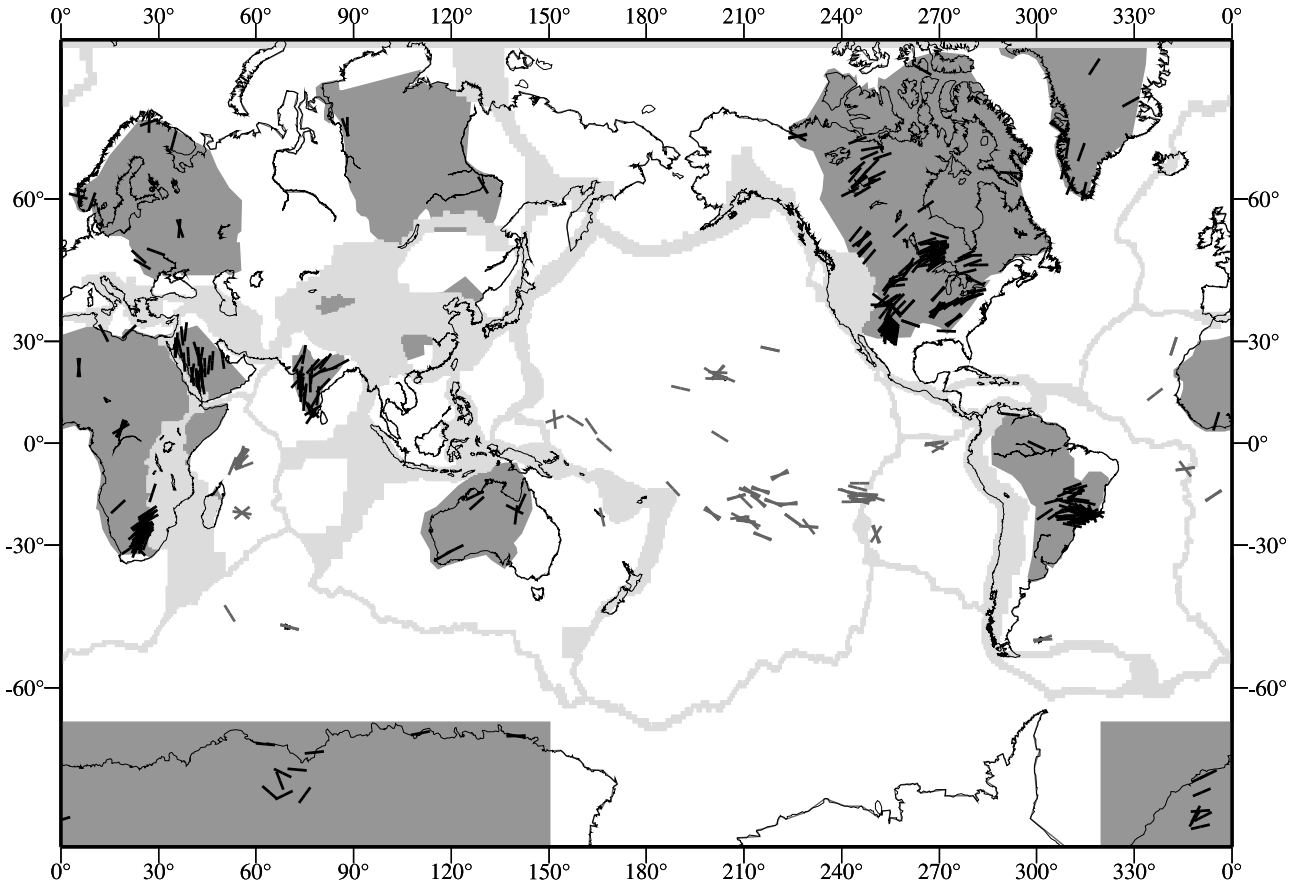

Figure 1. Compilation of shear wave splitting orientations for oceanic and cratonic areas (gray and black bars, respectively). Data is summarized in the auxiliary material. No data are used from plate boundary zones (light gray areas [*Kreemer et al.*, 2003]). For continents, data are only used from cratons (dark gray areas [*Artemieva and Mooney*, 2002; *Ritzwoller et al.*, 2001]).

[18] To obtain an APM model using the φ_{SKS} data, a model of relative plate motions is required. It is most intuitive (but not necessary) to have the input velocities expressed in an NNR frame, because then I can directly invert for the net rotation of the lithosphere that best fits the φ_{SKS} data. I therefore use the plate motions predicted by the NNR model of *Kreemer et al.* [2006] (GSRM-NNR-2), which is mainly based on geodetic velocities of relative present-day plate motions, but has the motions of a few small oceanic plates constrained by published estimates based on seafloor data. (None of the SKS data is on those small plates.) The most important reason for using GSRM-NNR-2 is that its NNR frame was estimated better than in earlier studies by taking into account the velocity gradient field in plate boundary zones [see also *Kreemer and Holt*, 2001]. In addition, GSRM-NNR-2 provides a better description of actual surface motions than geological models such as NUVEL-1A [*Argus and Gordon*, 1991; *DeMets et*

Table 1. Net Rotation of Entire Lithosphere Relative to Lower Mantle, and Data Misfit, for Models Using Different Data Input

	Rotation Vector[a] (°/Ma)			NRMS/Average Misfit[b] (°)													
Data	ω_x	ω_y	ω_z	all	oc	cr	an	ar	au	eu	in	na	nu	nz	pa	sa	so
All	0.0499	0.0988	−0.1743	5.3 23	5.4	5.2 24	7.2 25	2.5	4.5	6.1	3.5	4.3	5.6	6.1	6.3	7.3	2.8
	(0.0002)	(0.0001)	(0.0006)		19			29	34	53	25	23	20	19	19	21	19
Ocean	0.0937	0.1032	−0.1351	7.4 24	5.4	8.0 26	22.1	2.6	4.4	5.8	3.6	5.0	6.5	5.9	6.2	8.2	3.0
	(0.0041)	(0.0039)	(0.0034)		20		56	31	34	50	26	22	15	22	19	25	20
Craton	0.0499	0.0988	−0.1743	5.3 23	5.4	5.2 24	7.2 25	2.5	4.5	6.1	3.5	4.3	5.6	6.1	6.3	7.3	2.8
	(0.0002)	(0.0001)	(0.0007)		19			29	34	53	25	23	20	19	19	21	19
Sub 1[c]	0.0618	0.1201	−0.1768	6.2 24	5.4	6.4 26	16.3	2.4	4.6	5.7	3.3	4.3	5.0	6.0	6.3	7.4	2.8
	(0.0022)	(0.0015)	(0.0011)		19		59	27	34	50	25	22	17	20	19	22	19
Sub 2[d]	0.1018	0.0654	−0.2717	11.4	7.1	12.4	37.2	2.7	5.6	5.7	2.7	4.2	17.2	5.8	6.1	7.2	6.7
	(0.0040)	(0.0110)	(0.0136)	30	30	30	94	23	38	47	23	22	52	28	19	21	38

[a]Values in parenthesis are 1 standard deviation.
[b]Data misfit are shown for all data (all), only oceans (oc) or cratons (cr) and for each plate individually (an, Antarctica; ar, Arabia; au, Australia; eu, Eurasia; in, India; na, North America; nu, Nubia; nz, Nazca; pa, Pacific; sa, South America; so, Somalia).
[c]Only data used on Nubian, Somalian, Arabian, Indian, and oceanic parts of Antarctic and South American plates to constrain rotation.
[d]Only data on Pacific, Nazca, and North American plates to constrain rotation.

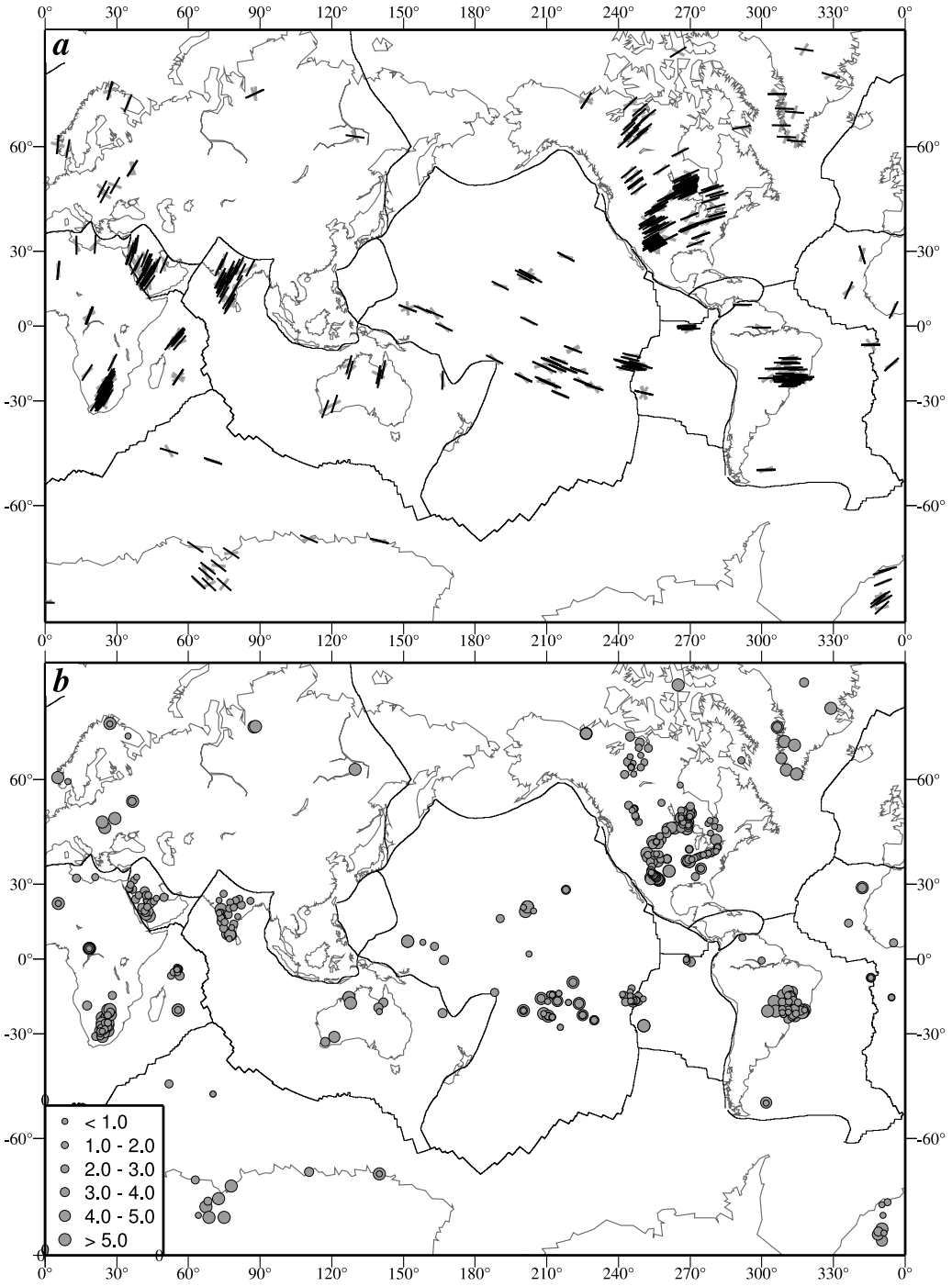

Figure 2. (a) Comparison of shear wave splitting orientations (gray bars) with predicted APM directions (black bars). (b) NRMS of misfit between shear wave splitting orientations and plate motion directions. Values per plate or per domain are summarized in Table 1.

al., 1994] by, for example, considering the African plate as two independent plates (Nubia and Somalia). By using the *Kreemer et al.* [2006] result, the APM model presented here implicitly includes velocity predictions for diffuse plate boundary zones. The latter would be useful for studies that investigate the dynamics of plate boundary zones using seismic anisotropy analysis. Because of the use of GSRM-NNR-2 as NNR and relative plate motion input, the preferred model presented below will be referred to as GSRM-APM-1.

[19] To align $\vec{v}_{APM}$ to N observations of φ_{SKS}, I minimize

$$\sum_{i=1}^{N}\left[\frac{\varphi_{SKS}-\tan^{-1}\left(v_{APM}^{long}/v_{APM}^{lat}\right)}{\sigma_{\varphi}}\right]^{2}, \qquad (1)$$

where $\vec{v}_{APM}$ is the sum of the velocity in the NNR frame and the velocity corresponding to a rigid body rotation $\vec{\omega}$ between the NNR frame and APM at the location of the

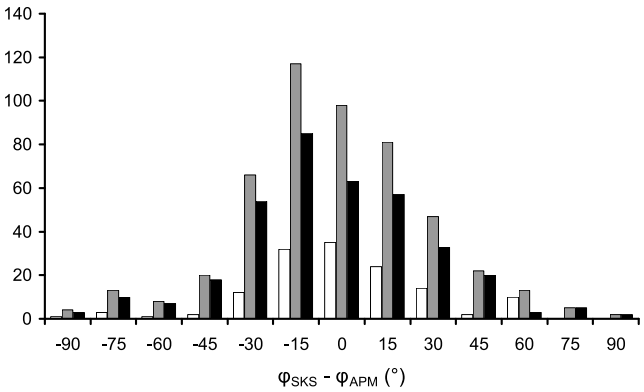

Figure 3. Histogram plot of misfit between shear wave splitting and APM directions for all data (gray bars), oceanic areas (white bars), and cratonic areas (black bars).

φ_{SKS} measurement. I solve for $\vec{\omega}$ with a nonlinear minimization scheme using the Levenberg-Marquardt method [*Press et al.*, 1992]. I use published standard deviations in φ_{SKS} (σ_φ) (set to 10° when unknown) and ignore uncertainties in the plate velocities, which are typically much less than those in φ_{SKS}. To overcome the 180° ambiguity between φ_{APM} and φ_{SKS}, all φ_{SKS} values were taken closest to the expected φ_{APM}.

4. Results

[20] Net rotation angular velocity vectors $\vec{\omega}$ and misfit statistics to the φ_{SKS} data are summarized in Table 1 for five different models, each considering a different set of φ_{SKS} values in determining $\vec{\omega}$. In the preferred model, GSRM-APM-1, all 474 available φ_{SKS} estimates are used. In the first two alternative models ("ocean" and "craton") only the 115 or 359 data values for oceanic or cratonic areas, respectively, are used. In another model ("Sub 1"), the data is limited to the 144 data values that come from only the Nubian, Somalian, Arabian, and Indian plates and oceanic portions of the Antarctic and South American plates. The result associated with this subset of data may provide an analog to those hot spot APM models that only use data from the Indo-Atlantic region [e.g., *Müller et al.*, 1993; *O'Neill et al.*, 2003]. Moreover, a model based on this subset of data would address the notion that the lithosphere's net rotation is constrained only by data from the Indo-Atlantic region. The final model ("Sub 2") uses only the 241 data points from the Pacific, Nazca, and North American plates, and could be considered an opposite model to Sub 1. A model based on only data from the Pacific, Nazca, and North American plates would be more akin to HS3-NUVEL1A, which (except for the orientation of the Martin Vaz hot spot track in South America) only uses data from hot spots on those three plates.

[21] For GSRM-APM-1, the best fitting net rotation of the lithosphere is described by an angular velocity vector whose x, y, and z components are 0.0499 ± 0.0002°/Ma, 0.0988 ± 0.0001°/Ma, and −0.1743 ± 0.0006°/Ma (uncertainties are one standard deviation), respectively. This angular velocity corresponds to a counterclockwise rotation of 0.2065°/Ma around an Euler pole at 57.58°S and 63.20°E. Globally, the average misfit between φ_{SKS} and φ_{APM} is 23° (normalized root-mean-square (NRMS) using published standard deviations is 5.3), and for oceans and cratons it is 19° and 24° (5.4 and 5.2 NRMS), respectively (Table 1). Figure 2 gives a visual depiction of the fit between data and model. Table 1 summarizes the misfits for individual plates. A histogram of the global average misfit (Figure 3) indicates that there is no strong bias in orientation, although the average misfit is slightly counterclockwise from zero (dominated by data from the Colorado Plateau, as well as the Somalian plate). The misfit for the North American plate would be smaller than reported here, if the Colorado Plateau area were considered part of the North America-Pacific plate boundary in the GSRM. There is now strong evidence from space geodetic data that the Plateau actively deforms [*Kreemer et al.*, 2008], and the area will be included as part of the plate boundary in future versions of the GSRM. For now, the Colorado Plateau is considered part of the North American craton [*Artemieva and Mooney*, 2002], and φ_{SKS} there is consistently ∼20°–50° counterclockwise from φ_{APM}.

[22] To illustrate that the net rotation of GSRM-APM-1 is a unique result, I calculate the misfit between φ_{SKS} and φ_{APM} for variable net rotation rates. For this, I keep the orientation of the net rotation axis similar to the one obtained, but vary the rotation rate from zero (i.e., NNR) to 0.5°/Ma (i.e., somewhat more than the 0.436°/Ma implied by HS3-NUVEL1A) (Figure 4). The net rotation of 0.2065°/Ma clearly minimizes the fit to the data. Data from oceanic islands may be equally well fit with a slightly larger net rotation. Globally, the misfit is 13° higher for a NNR case than for GSRM-APM-1, and 24° higher if one takes the net rotation of HS3-NUVEL1A (consistent with the findings of *Becker* [2008]). The results also clearly show

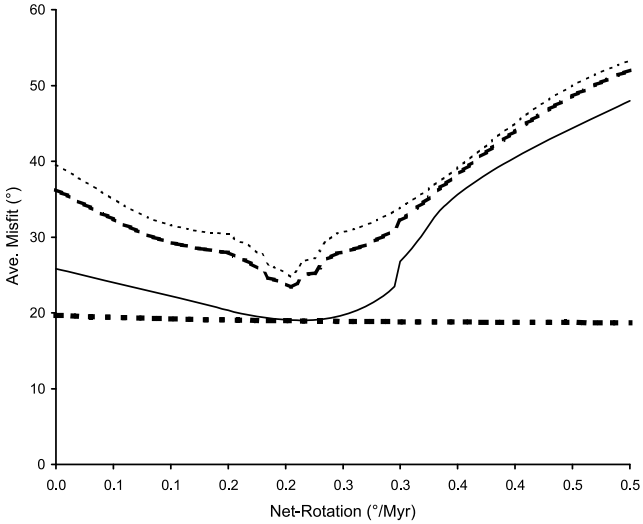

Figure 4. Globally averaged misfit between shear wave splitting and APM directions versus an assumed variable net rotation for the lithosphere relative to the mesosphere. Only the rate of net rotation is varied and the orientation of the rotation axis is held fixed from the preferred model (which corresponds to a rate of 0.2065°/Ma). Thick dashed line is misfit for all data, thin dotted line is misfit for data on cratons, solid line is misfit for oceanic data, and thick dotted line is misfit for data from the Pacific plate only.

that data on the Pacific plate do not constrain the net rotation rate. This insensitivity to Pacific data is because φ_{SKS} estimates there are aligned with the net rotation direction.

[23] An indistinguishable result from GSRM-APM-1 is obtained if only data from cratons are used (Table 1). A very similar result to GSRM-APM-1 is also found for the model based on data in the Indo-Atlantic region (Sub 1), with the globally averaged misfit only 1° worse than for GSRM-APM-1. On the other hand, a significantly different net rotation is obtained if only data from ocean islands or the Pacific, Nazca, and North American plates (Sub 2) are used. The average fit between φ_{SKS} and φ_{APM} in the latter two models is, however, not significantly better for the areas or plates from which the data are used than for any of the other models, while the globally averaged misfit is significantly larger (Table 1). When data is limited only to the Pacific, Nazca, and North American plates, the global misfit (for all data or only those at cratons or oceanic islands) is the worst. Instead, when only data from the Indo-Atlantic region are used, a similar net rotation (and data misfit) is found than when all data are used, supporting the idea that the net rotation is constrained by the indicators of φ_{APM} in this part of the world and not by those in the Pacific region.

[24] The data is globally very heterogeneously distributed, and the models could be biased due to a preferred fit in regions with high data density. To investigate this effect, an alternative model was determined that exclude data from the North America, India and Arabia (the three plates with highest data density). For this model (which has 257 data points) the x, y, and z components of the rotation vector are 0.0497 ± 0.0002°/Ma, 0.0988 ± 0.0001°/Ma, and -0.1734 ± 0.0007°/Ma. This result is indistinguishably different from the preferred model, and yields an identical data misfit. I thus conclude that data density variation does not bias the inversion and does not warrant a weighted inversion scheme.

[25] The GSRM-APM-1 Euler poles for all plates are determined by combining the net rotation angular velocity with those of each plate in the NNR frame [*Kreemer et al.*, 2006] (values are listed in Table 2). The uncertainty in the plate rotations is dominated by the uncertainty in the relative plate motions, which are listed by *Kreemer et al.* [2006]. Table 2 also lists the average, minimum, and maximum velocities for each plate, as well as those associated with the net rotation of the entire lithosphere. Figure 5 shows the velocities corresponding to the plate rotations, and the velocities in plate boundary zones. The slowest moving large plates are Antarctica, Eurasia, and Nubia. All three plates have large cratonic areas and negligible or no subducting slab attached to it. Some small oceanic plates that are not attached to a subducting slab (Caribbean, Scotia, Okhotsk) move very slowly as well. The motion of all plates is significantly different than earlier estimates and is generally between that predicted by HS3-NUVEL1A and those predicted by models based on hot spot trends alone: "MPM07" by *Morgan and Phipps Morgan* [2007] and T22A [*Wang and Wang*, 2001]. For example, GSRM-APM-1 predicts 85.4 mm/a for Hawaii (Pacific plate), whereas HS3-NUVEL1A predicts 103.3 mm/a, MPM07 80.0 mm/a, and T22A 83.0 mm/a. For Easter Island (Nazca Plate), GSRM-APM-1 predicts 42.6 mm/a, HS3-NUVEL1A 32.7 mm/a, MPM07 61.0 mm/a, and T22A 65.9 mm/a. For Yellowstone (North American plate), GSRM-APM-1 predicts 23.0 mm/a, HS3-NUVEL1A 26.8 mm/a, MPM07 17.0 mm/a, and T22A 22.1 mm/a.

5. Comparison With Hot Spot Tracks

[26] To test the compatibility of GSRM-APM-1 with hot spot track data, I use the compilation of recent (e.g., mostly <5–10 Ma, but for some ~30 Ma) hot spot track parameters by *Morgan and Phipps Morgan* [2007]. Their data set consists of azimuth estimates φ_{HS} for 59 hot spots, and full velocity estimates $\vec{v}_{HS}$ for 34 of those. Figure 6 shows the comparison between φ_{APM} and φ_{HS}, and summarizes the misfit statistics for each plate. The average plate misfit is <8° for hot spots on the Pacific, Nazca, Australian, South America, and North American plates (the latter excluding Iceland and Azores, which are in plate boundaries where GSRM velocities do not indicate rigid plate motion). But for hot spots on Antarctica, Eurasia, and Africa (combining Nubia and Somalia), the average misfits are large and can vary significantly between hot spots. For example, the misfit for neighboring Ob-Lena and Crozet hot spots on the Antarctic plate is <2°, but is >25° for all other Antarctic hot spots. Similarly the fit is poor for Eifel (65°), but good for Baikal (5°), the only other hot spot on the stable Eurasian plate. Despite these variations, there is a clear global correlation between $\vec{v}_{APM}$ and the goodness of fit between φ_{APM} and φ_{HS} (Figure 7).

[27] It is unsurprising to find relatively large misfits for hot spots on slow-moving plates. First, small motions of the lower mantle can affect plume motion (see section 6) and thus hot spot tracks (azimuth and rate) when the plate is slow. Second, complex interactions between the plume and lithosphere are more common for slow plates and can obscure the hot spot track's reflection of φ_{APM}. Third, for slow plates, φ_{HS} is occasionally derived from a relatively old (~30 Ma) progression of volcanic centers that may not reflect the most recent φ_{APM} if plate motion has changed. Moreover, the rotation pole of some plates is located inside the plate (e.g., Antarctica and Nubia), very near to some of the hot spots, and thus any small uncertainty in the pole location could significantly change the expected φ_{APM}. This effect could, for example, partly explain the large misfits for the Nubian hot spots in the mid-Atlantic.

[28] To test the consistency between φ_{APM} and φ_{HS} in a different way, I compare φ_{APM} predictions of GSRM-APM-1 with 11 recent (i.e.,< 5 Ma) hot spot azimuths used in HS3-NUVEL1A [*Gripp and Gordon*, 2002]. The average misfit per plate is smaller for GSRM-APM-1 than HS3-NUVEL1A for all four plates where *Gripp and Gordon* [2002] estimated hot spot azimuths (Pacific, Nazca, North America, and South America). That is, the misfit for the Pacific hot spots is 6.8° using φ_{APM} from GSRM-APM-1 versus 7.0° when using HS3-NUVEL1A. The misfits are 19.2° versus 19.9° for Nazca, 2.6° versus 8.5° for North America, and 5.3° versus 13.7° for South America, respectively. I conclude that GSRM-APM-1 fits the hot spot tracks of *Gripp and Gordon* [2002] better than HS3-NUVEL1A itself, because the velocities in HS3-NUVEL1A were also constrained to match the rates of the Hawaiian and Society tracks. Those rates are likely affected by mantle flow (see below), which would skew the entire model (in rate and direction). As a conse-

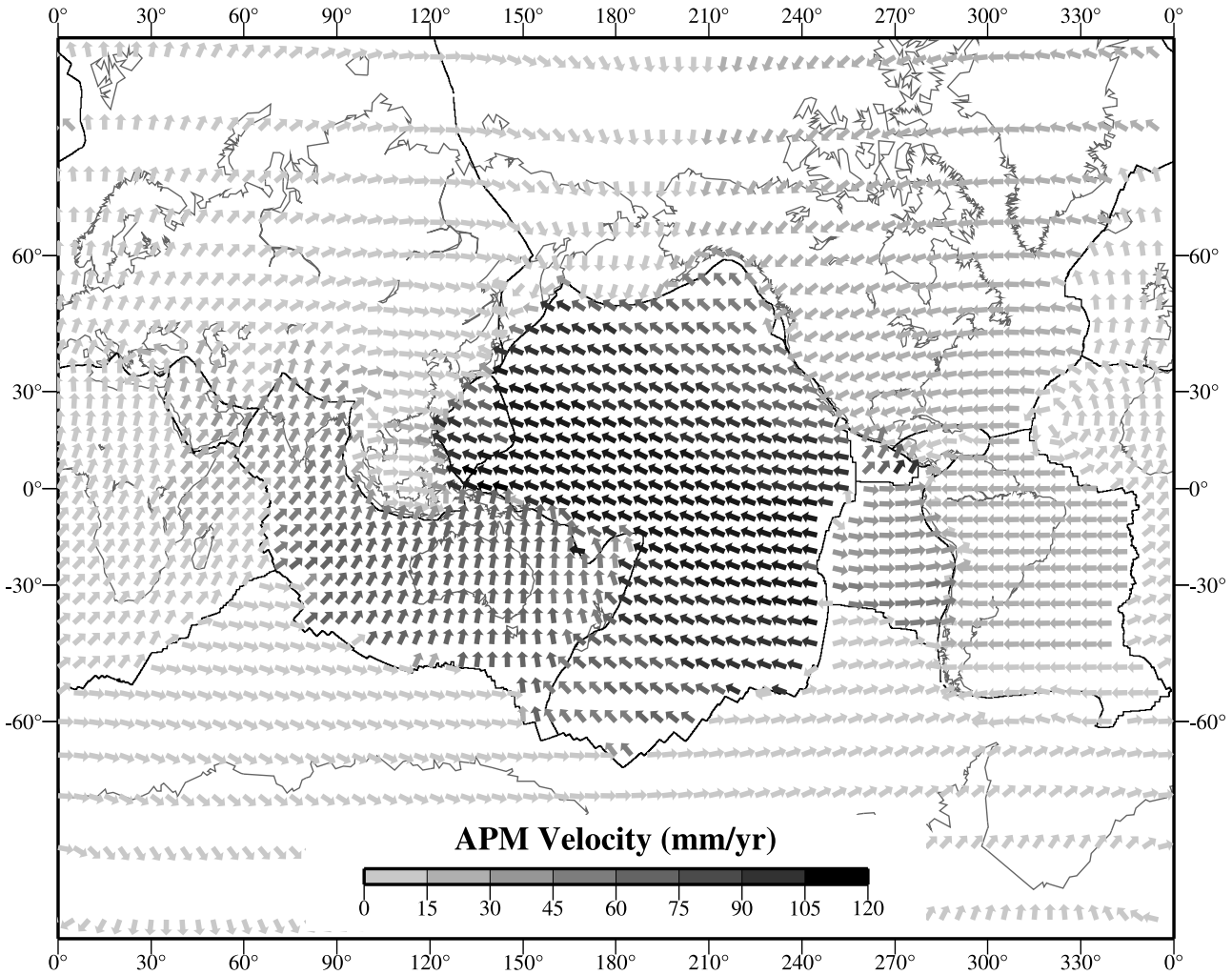

Figure 5. Global velocity field in GSRM-APM-1 reference frame. Euler poles that describe rigid plate motions are listed in Table 2. Note that GSRM-APM-1 also describes the motions for the (diffuse) plate boundary zones.

quence, velocities in the HS3-NUVEL1A will increasingly misfit hot spot track data with distance from the Pacific plate. In the extreme cases of Eurasia and Nubia, HS3-NUVEL1A velocities are roughly opposite in direction to observed φ_{HS}, as noted earlier by *Morgan and Phipps Morgan* [2007].

[29] For the 34 hot spots where $\vec{v}_{HS}$ is known (here defined to be oriented from older to younger volcanic centers) [*Morgan and Phipps Morgan*, 2007], the motion of hot spots (i.e., the underlying plume) in the GSRM-APM-1 frame ($\vec{v}_{plume}$) can be determined by adding $\vec{v}_{HS}$ to $\vec{v}_{APM}$ (Table 3). Figure 8 shows $\vec{v}_{plume}$ for all hot spots where $\vec{v}_{plume}$ is outside the 95% uncertainty in $\vec{v}_{HS}$. The large and anomalously oriented motion of the Comores and Marquesas plumes can be traced back to anomalous φ_{HS}, possibly indicating complex interaction between a shallow plume source and the lithosphere [cf., *Morgan and Phipps Morgan*, 2007].

[30] For the majority of hot spots with significant plume velocities, $\vec{v}_{plume}$ is typically (much) smaller than $\vec{v}_{APM}$ and, because $\vec{v}_{HS}$ is larger than $\vec{v}_{APM}$, $\vec{v}_{plume}$ is antiparallel to $\vec{v}_{APM}$. Moreover, near spreading ridges, $\vec{v}_{plume}$ is typically oriented toward the ridge. Past comparisons between previous $\vec{v}_{APM}$ estimates and $\vec{v}_{HS}$ concluded that the difference between $\vec{v}_{HS}$ and $\vec{v}_{APM}$ can be explained by lower-mantle flow antiparallel to the plate motion [*Wang and Wang*, 2001; *Wang and Liu*, 2006; *Morgan and Phipps Morgan*, 2007]. However, any such inference relies on the assumption that the plume originates in the lower mantle. Because this is not always the case [e.g., *Zhao*, 2001; *Courtillot et al.*, 2003; *Montelli et al.*, 2006; *Boschi et al.*, 2007], I discuss in section 6 various mantle flow scenarios that could explain $\vec{v}_{plume}$ for different plume depth origins, and apply these ideas to the observations.

6. Implications for Mantle Flow

[31] Figure 9 summarizes seven simple 2-D scenarios of horizontal mantle flow, given the observed difference in $\vec{v}_{APM}$ and $\vec{v}_{HS}$ and the depth of the plume. In all these cases, $\vec{v}_{APM}$ and $\vec{v}_{HS}$ are assumed to be generally antiparallel (given my definition of $\vec{v}_{HS}$). In case A, $v_{HS} > v_{APM;}$ in case B, $v_{HS} = v_{APM}$ (within 95% confidence interval of $\vec{v}_{HS}$); and in case C, $v_{HS} < v_{APM}$. In all cases, $\vec{v}_{plume}$ equates to mantle flow at the top of the mesosphere for a hot spot with a deep

Table 2. Plate Euler Poles and Velocities of GSRM-APM-1[a]

Plate	Latitude (°N)	Longitude (°E)	$\dot{\omega}$ (°/Ma)	v_{ave} (mm/a)	v_{min} (mm/a)	v_{max} (mm/a)
Amur	71.0	−99.3	0.097	9.2	8.3	9.9
Anatolia	33.6	29.5	1.331	15.1	9.3	21.2
Antarctica	77.6	−179.9	0.031	1.6	0.0	2.9
Arabia	33.6	12.6	0.472	27.6	17.6	37.3
Australia	15.6	40.3	0.643	66.4	43.8	71.5
Capricorn	20.5	41.5	0.672	57.8	47.2	66.4
Caribbean	2.5	−70.7	0.128	3.4	2.4	5.0
Caroline	−60.9	−3.7	1.054	105.3	101.3	108.8
Cocos	20.8	−117.0	1.335	62.6	31.2	89.0
Eurasia	42.0	−60.9	0.078	7.0	3.1	8.9
India	32.9	9.3	0.430	42.1	35.6	46.7
Juan de Fuca	−41.4	57.7	1.562	17.5	8.6	24.7
Nazca	41.0	−93.1	0.426	40.9	29.1	47.3
North America	−52.4	−53.0	0.218	20.6	7.1	24.3
Nubia	20.8	−39.1	0.123	9.6	0.0	13.7
Okhotsk	−56.9	−34.2	0.462	5.3	0.2	10.9
Pacific	−64.1	96.2	0.849	84.2	41.5	94.4
Philippine Sea	−55.5	−13.5	0.981	77.3	55.1	96.3
Rivera	18.8	−106.6	4.361	15.5	3.8	26.1
Scotia	−71.2	−51.1	0.193	5.5	4.1	6.9
Somalia	38.6	−66.7	0.156	15.0	11.0	17.2
South America	−89.1	22.1	0.203	20.1	11.4	22.6
South China	78.2	−72.5	0.140	14.5	13.9	14.9
Sunda	27.2	−72.5	0.210	13.1	8.1	17.5
Tarim	−30.8	−82.9	0.518	13.9	10.5	17.3
Lithosphere	−57.6	63.2	0.207	18.1	0.0	23.0

[a]Euler poles describing rotations relative to the subasthenospheric mantle and the corresponding average, minimum, and maximum velocities of all plates (and lithosphere as a whole). Relative plate motions are from *Kreemer et al.* [2006].

mantle source, if the plume head has reached the surface (and thus is in steady state) [e.g., *Steinberger*, 2000; *Steinberger et al.*, 2004].

[32] When case A is satisfied for a hot spot whose plume source is below the asthenosphere, $\vec{v}_{plume}$ indicates subasthenospheric counterflow at the top of the mesosphere. In this scenario, there may be either simple channel flow in the asthenosphere itself (i.e., the simplest assumption) or asthenospheric counterflow (case A1 or A2, respectively). For case A, $\vec{v}_{plume}$ indicates lower-asthenospheric counterflow (or "return flow"), when the plume source is the lower asthenosphere (case A3).

[33] The simplest scenario to explain case B considers a plume that originates in a static subasthenospheric mantle (case B1). Case B can also be satisfied if the plume source is middepth in an asthenosphere undergoing return flow (case B2). To satisfy case C when the source is deep, an amount of subasthenospheric mantle flow is required in the direction of $\vec{v}_{APM}$ (case C1). Alternatively, the source could be within an asthenosphere undergoing simple channel flow (case C2).

[34] The above examples do not consider the possibility of asthenospheric or lower mantle flow that is significantly oblique to φ_{APM}, in which case many more models are possible than the few flow hypotheses discussed here. I do not consider scenarios for which $\vec{v}_{HS}$ is parallel (as opposed to antiparallel) to $\vec{v}_{APM}$, which would require $\vec{v}_{plume}$ to be faster than $\vec{v}_{APM}$. If the plume source is below the asthenosphere, such scenarios would imply that the lower mantle moves faster than the surface (i.e., mantle "leading" the lithosphere). I do not observe a case of the mantle leading the lithosphere in the existing hot spot data set.

[35] Even now that source depths are relatively well known [e.g., *Zhao*, 2001; *Courtillot et al.*, 2003; *Montelli et al.*, 2006; *Boschi et al.*, 2007; *Zhao*, 2007], equating $\vec{v}_{plume}$ to mantle flow is complicated by the possibility of having various combinations of subasthenospheric and asthenospheric flow mechanisms. Therefore, I propose a mantle flow scenario exclusive to hot spots (see below) where (1) independent flow predictions are known or (2) the plume originates within the asthenosphere (and is thus unaffected by flow in the mesosphere).

[36] For Hawaii, there is a significant $\vec{v}_{plume}$ of 12.4 mm/a toward S1°E. Because the plume originates in the deep mantle, $\vec{v}_{plume}$ signifies flow at the top of the mesosphere (case A1). This estimate is extremely close to that predicted from one of the density-driven convection models of *Steinberger* [2000] (i.e., 13 mm/a toward S36°E, when using the tomographic model of *Su et al.* [1994] with the plume source at 670 km). My estimate of $\vec{v}_{plume}$ is also very close in magnitude and direction to Hawaiian hot spot motion during the Cenozoic, as inferred from plate reconstructions and paleomagnetic investigations [e.g., *Molnar and Stock*, 1987; *Tarduno et al.*, 2003]. My result suggests that the lithosphere is leading the mantle through simple asthenospheric channel flow, with oblique counterflow at the top of the mesosphere that is ~1/7 of the magnitude of $\vec{v}_{APM}$.

[37] At St. Helena, $\vec{v}_{plume}$ is 12.0 mm/a toward the Mid Atlantic Ridge (N79°W). Because its plume appears to originate in the lower asthenosphere, I propose that $\vec{v}_{plume}$ reflects asthenospheric return flow (case A2). The hypothesis of return flow near the Mid Atlantic Ridge is supported by $\vec{v}_{plume}$ being notably close to $-\vec{v}_{APM}$ in both magnitude and direction ($\vec{v}_{APM}$ is 10.0 mm/a toward N39°E). It should be noted, however, that *Steinberger*'s [2000] predicted motion of a hypothetical deep plume would be roughly similar to $\vec{v}_{plume}$ for St. Helena. This correlation suggests that asthenospheric return flow and subasthenospheric counterflow may be roughly equal.

[38] For Easter hot spot, which has a deep plume origin, my model predicts a large $\vec{v}_{plume}$ toward the East Pacific Rise (53.3 mm/a toward S76°W). This motion is much larger than the 10 mm/a of predicted flow at the top of the mesosphere [*Steinberger*, 2000]. An additional asthenospheric return flow component of ~43 mm/a is thus required to explain $\vec{v}_{plume}$ (combination of cases A2 and A3). This predicted amplitude of asthenospheric return flow is exactly equal (but antiparallel) to $\vec{v}_{APM}$.

[39] There is still debate on the depth of the Galápagos plume [e.g., *Courtillot et al.*, 2003; *Montelli et al.*, 2006; *Zhao*, 2007], but it appears to originate beneath the transition zone [*Hooft et al.*, 2003]. The inferred $\vec{v}_{plume}$ of 24.3 mm/a toward N74°W is therefore most easily explained as flow in the upper mesosphere toward the East Pacific Rise (case A1), and is consistent with the estimates of *Steinberger* [2000]. Located >1000 km from the East Pacific Rise, no asthenospheric return flow is required underneath Galápagos.

[40] For Kerguelen, which has a deep mantle source, $\vec{v}_{plume}$ is insignificant (case B1), consistent with the latest mantle flow prediction [*Steinberger and Antretter*, 2006]. At Réunion island, $\vec{v}_{plume}$ is 30.4 mm/a toward S46°W, roughly antiparallel to $\vec{v}_{APM}$ (5.8 mm/a toward N42°E). The Réunion

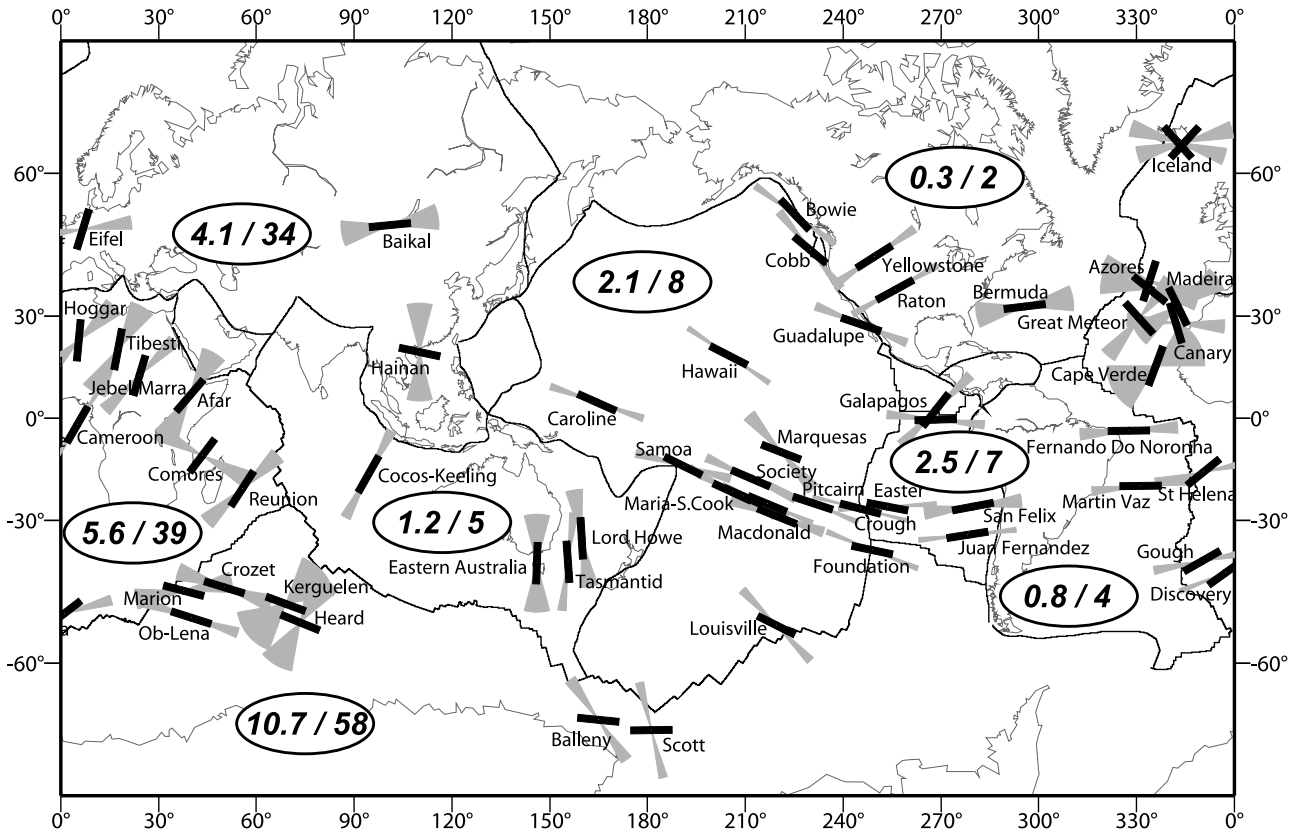

Figure 6. Hot spot propagation azimuths and their 1σ uncertainties (gray wedges) from *Morgan and Phipps Morgan* [2007] and APM orientations (black bars). The average misfit and NRMS misfit are shown for each plate with hot spots. For these statistics, misfits for the "plate boundary" hot spots (Iceland, Azores, and Hainan) are excluded.

plume has a deep origin, but $\vec{v}_{plume}$ is much larger than predicted by the models of *Steinberger* [2000]. Moreover, $\vec{v}_{plume}$ is antiparallel to the more recently predicted small NNE-directed motion [*O'Neill et al.*, 2003]. In any case, $\vec{v}_{plume}$ below Réunion can only be explained by asthenospheric return flow that is ~5 times faster than v_{APM}.

[41] For Louisville and Foundation, v_{HS} is less than v_{APM} (i.e., case C). At the same time, $\vec{v}_{plume}$ is highly oblique to $\vec{v}_{APM}$ and parallel to the Pacific-Antarctic ridge. Because the Louisville plume source is deep, I speculate that ridge-parallel asthenospheric flow (proposed to occur there by *Marks and Stock* [1994]) could be responsible for the anomalous $\vec{v}_{plume}$.

[42] For Yellowstone, I find $\vec{v}_{plume}$ to be insignificant. Because the plume originates within the midasthenosphere [*Christiansen et al.*, 2002; *Yuan and Dueker*, 2005; *Waite et al.*, 2006], asthenospheric counterflow could explain the correlation of the hot spot propagation vector with the GSRM-APM-1 velocity prediction (case B2). This result is consistent with the finding by *Becker et al.* [2006] that counterflow is expected at ~300 km depth. Modeling predictions suggest a significant component of counterflow at the top of the mesosphere as well [*Steinberger*, 2000; *Silver and Holt*, 2002; *Moucha et al.*, 2008]. The models by *Steinberger* [2000] predict an amplitude and direction of lower-mantle flow close to $-\vec{v}_{APM}$.

[43] Although the depth of the Raton plume is not well known [*Courtillot et al.*, 2003; *Zhao*, 2007], and the underlying flow field can thus not be constrained by my approach, it should be noted that, like Yellowstone, its $\vec{v}_{APM}$ is of similar amplitude and antiparallel with the model predictions of *Steinberger* [2000].

[44] Besides Yellowstone and Raton, Eifel is the only other continental hot spot for which $\vec{v}_{plume}$ can be estimated.

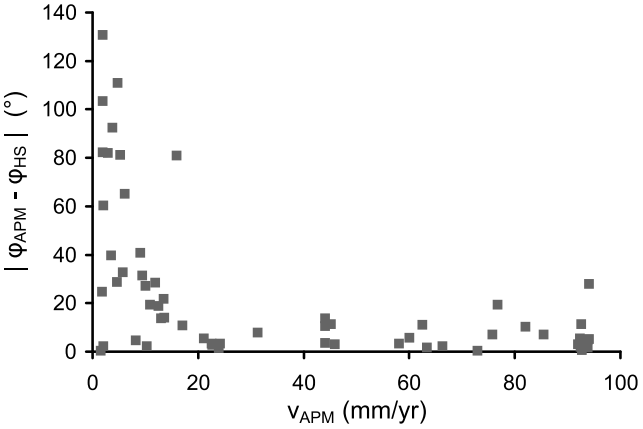

Figure 7. Absolute misfit between hot spot track azimuths and APM directions versus APM velocity. The large misfits are uniquely coming from the slow moving plates (<15 mm/a).

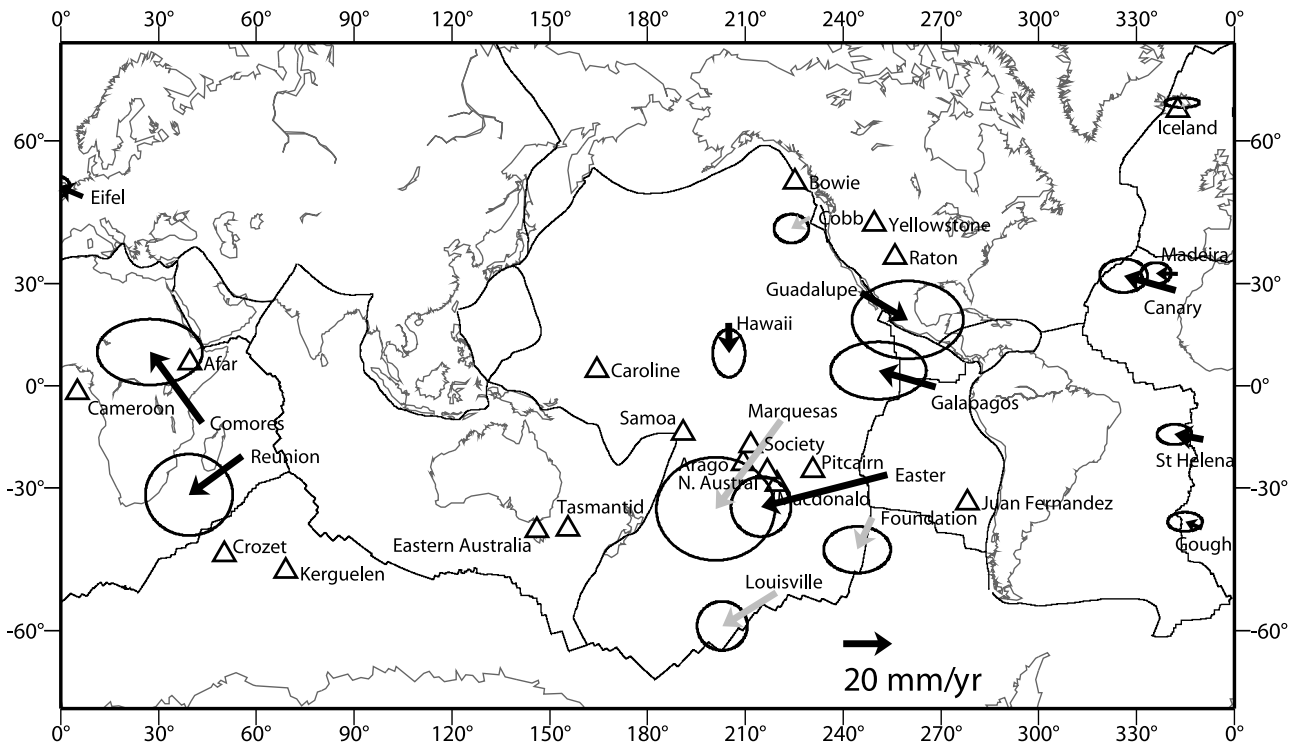

Figure 8. For all hot spots with known propagation rates [*Morgan and Phipps Morgan*, 2007], the motion of the hot spot (i.e., that of its underlying plume) relative to the mesosphere is determined by adding the observed hot spot propagation vector (defined from old to new volcanic centers) to the predicted APM velocity (Table 3). When the hot spot propagation is faster than APM, the plume velocity is shown as a black vector, and when the hot spot propagation is slower than APM, the plume velocity is shown as a gray vector. Error ellipses represent 95% confidence interval of the observed track propagation vectors. When hot spot and APM velocity are equal (within 95% confidence) a triangle instead of a vector is shown.

Its significant motion of 11 mm/a toward N67°W is almost perpendicular to $\vec{v}_{APM}$ (6.2 mm/a toward N17°E). There is no evidence that the plume originates below 400 km [*Ritter et al.*, 2001; *Pilidou et al.*, 2005] and $\vec{v}_{plume}$ would indicate asthenospheric motion in my simple hypotheses. Mantle and asthenospheric flow models are, however, particularly inconclusive on the expected flow in this region. The predicted flow depends strongly on which tomographic model is used, and whether a regional or global model is considered [*Steinberger*, 2000; *Marquart et al.*, 2007]. This uncertainty in expected flow, plus the obliquity between φ_{plume} and φ_{APM}, make it difficult to place the predicted $\vec{v}_{plume}$ in the context of mantle flow. The difficulty of relating $\vec{v}_{plume}$ to mantle flow is compounded by the fact that there is considerable uncertainty in $\vec{v}_{HS}$. The estimate of $\vec{v}_{HS}$ for the Eifel hot spot by *Morgan and Phipps Morgan* [2007] is valid for volcanic centers between 17 and 22 Ma. This old-to-young westward propagation is roughly antiparallel to the most recent propagation of volcanic centers (0.5–2.7 Ma [*Illies et al.*, 1979]). An eastward old-to-young propagation would be more consistent with that inferred from the regional φ_{SKS} pattern [e.g., *Walker et al.*, 2005] (not used in this study). However, an opposite $\vec{v}_{HS}$ would not, by itself, predict a $\vec{v}_{plume}$ that is more consistent with flow predictions. Although $\vec{v}_{APM}$ is very different from previous estimates (and, if wrong, could be the cause of the anomalous $\vec{v}_{plume}$), independent evidence of shallow, APM-controlled, tilting of the Eifel plume toward the NNE [*Wüllner et al.*, 2006] suggests that GSRM-APM-1 properly describes $\vec{v}_{APM}$ in Europe (albeit some mm/a slower than *Wüllner et al.* [2006] found).

7. Discussion

7.1. Observed φ_{SKS} Versus Predicted φ_{APM}

[45] Misfits between φ_{SKS} and GSRM-APM-1's φ_{APM} predictions are generally small for oceanic plates, with NRMS for individual measurements often <2.0 (Figure 2). This consistency suggests that anisotropy in the oceanic asthenosphere can be explained by lithosphere-mesosphere differential motion, and strongly suggests a causal relationship between absolute plate motion and φ_{SKS}. The average misfit for oceanic areas of 19° is larger than the 13° found by *Conrad et al.* [2007] in a global comparison of φ_{SKS} and predicted LPO. However, the analysis presented here uses many more φ_{SKS} observations than *Conrad et al.* [2007], particularly for slow-moving plates, and does not exclude any observations in the misfit calculation. Consequently, most of the difference in the misfits found by me and *Conrad et al.* [2007] likely comes from oceanic areas of slow-moving plates, where density-driven flow has a proportionally larger effect on φ_{SKS}. This conclusion is supported by a comparison with the φ_{SKS} values reported by *Behn et al.* [2004] for oceanic areas around Africa. There, I

Table 3. Hot Spot Velocities v_{plume} in APM Frame[a]

Plate	Longitude (°E)	Latitude (°N)	v_{hs}^{lon} (mm/a)	v_{hs}^{lat} (mm/a)	σ_{hs}^{lon} (mm/a)	σ_{hs}^{lat} (mm/a)
Afar	39.5	7.0	3.1	−0.9	4.0	6.9
Arago	−150.7	−23.4	23.5	−14.7	18.0	8.8
Bowie	−134.8	53.0	1.9	8.5	2.6	4.2
Cameroon	5.1	−2.0	−2.8	−3.8	2.6	4.2
Canary	−18.0	28.2	−21.3	6.0	4.0	2.8
Caroline	164.4	4.8	41.7	−5.7	18.9	8.9
Cobb	−130.1	46.0	−7.7	−4.6	2.9	2.4
Comores	43.3	−11.5	−21.3	29.1	8.8	5.5
Crozet	50.2	−46.1	−21.7	7.5	12.3	4.2
Easter	−106.5	−26.4	−51.6	−13.2	5.0	5.0
Eastern Australia	146.0	−40.8	2.3	1.3	17.4	3.0
Eifel	6.7	50.2	−10.1	4.2	2.0	1.7
Foundation	−111.1	−37.7	−6.1	−13.1	5.6	3.9
Galapagos	−91.6	−0.4	−23.4	6.7	8.0	4.8
Gough	−10.0	−40.3	−6.8	2.8	2.9	1.6
Guadalupe	−114.5	27.7	19.1	−11.3	9.3	6.5
Hawaii	−155.2	19.0	0.2	−12.4	2.7	4.0
Iceland (Eurasia)	−15.3	64.4	−0.9	3.0	2.9	0.8
Iceland (North America)	−17.3	64.4	8.0	2.7	4.8	2.5
Juan Fernandez	−81.8	−33.9	−34.2	−1.3	19.9	4.2
Kerguelen	69.0	−49.6	−0.4	−2.6	1.1	1.3
Louisville	−140.6	−53.6	−22.0	−13.7	4.2	4.1
MacDonald	−140.3	−29.0	14.0	0.2	9.5	10.4
Madeira	−17.3	32.6	−8.9	0.2	2.5	1.8
Marquesas	−139.0	−10.5	−26.8	−36.4	9.9	8.6
North Austral	−143.3	−25.6	−16.6	6.2	13.8	5.9
Pitcairn	−129.3	−25.4	−6.2	−5.8	13.8	5.9
Raton	−104.1	36.8	5.0	3.5	17.3	10.0
Reunion	55.7	−21.2	−21.8	−15.9	7.3	6.8
Samoa	−169.1	−14.5	8.7	16.4	19.3	8.0
Society	−148.4	−18.2	12.6	−8.9	9.1	8.6
St. Helena	−9.5	−16.5	−11.8	2.2	2.9	1.7
Tasmantid	155.5	−40.4	−12.1	−0.2	5.5	5.0
Yellowstone	−110.4	44.5	2.1	2.7	4.1	2.9

[a]Hot spot velocities v_{plume} are determined from adding the APM velocity of the plate on which hot spot is located v_{APM} to the hot spot propagation vector v_{HS} (the latter defined as oriented from old to young volcanic centers) given by *Morgan and Phipps Morgan* [2007]. Figure 7 shows velocities only for hot spots where v_{plume} is more than the 95% uncertainty in v_{HS} [*Morgan and Phipps Morgan*, 2007].

find an average misfit of 24° (when excluding plate boundary sites ASI, HOPE, and CMLA, for which GSRM does not predict rigid plate motions but boundary motions instead). This misfit is equal to or better than any of their reported misfits, except for a model that considers plate-driven and density-driven flow simultaneously, for which they found a misfit of 13°.

[46] The average misfit between φ_{SKS} and φ_{APM} is globally ∼5° larger for cratons than for oceans. However, globally the NRMS is smaller for cratons than oceans due to the larger uncertainties in φ_{SKS} measurements on continents. NRMS values are particularly small for some cratons (e.g., India, Arabia, Australia) (Table 1). Still, large differences between φ_{SKS} and φ_{APM} exist for some cratons (e.g., Australia, Greenland, eastern Europe). There, φ_{SKS} must be either controlled by large anisotropy in the lithosphere and/or by significant density-driven flow in the asthenosphere. For example, Australia falls in the first category because asthenospheric anisotropy there is aligned to APM [*Simons and van der Hilst*, 2003; *Debayle et al.*, 2005], while anisotropy in the crust and lithosphere is controlled by frozen fabric [e.g., *Clitheroe and van der Hilst*, 1998; *Simons and van der Hilst*, 2003; *Heintz and Kennett*, 2005]. Given the apparent significance of lithospheric anisotropy, it could be argued that no φ_{SKS} data on cratons should be used in estimating APM. However, I show that models based on oceanic data alone lead to larger misfits at cratons, while not having an improved data fit at the oceanic stations. Moreover, a model that only uses data on cratons gives a nearly identical net rotation to a model that uses all data. Thus, although possible affected by lithospheric anisotropy, cratonic data provides important constraints when inferring APM on a global scale.

7.2. Absolute Plate Motions

[47] GSRM-APM-1 velocities are generally slower than those predicted by HS3-NUVEL1A. In terms of direction, the velocities between the two models are similar for the "Pacific hemisphere," with motions trending toward subduction zones and away from ridges (Figure 5). These characteristic motions are expected [*Gordon et al.*, 1978] for plates controlled by slab-pull and (to lesser extent) ridge-push [e.g., *Forsyth and Uyeda*, 1975; *Harper*, 1975; *Solomon et al.*, 1975]. For the "Indo-Atlantic" hemisphere, however, there are significant differences in direction between the two APM models. Unlike HS3-NUVEL1A, GSRM-APM-1 velocities are directed toward the subduction/convergence zones north of the Nubian, Arabian, and Indian plates. In this sense, GSRM-APM-1 is more like the hot spot models based on tracks in the Indo-Atlantic domain (particularly if plumes are allowed to move with mantle flow) [*O'Neill et al.*, 2003]. Interestingly, I observe that my model's rotation poles for Arabia and India fall within ∼3° of each other in the western Mediterranean. The location and closeness of the poles suggest that the motion of both plates is (still) driven by the same process: the subduction that closed the Tethys Ocean.

[48] In GSRM-APM-1, the slowest plate is Antarctica, whose velocity does not exceed 3 mm/a (Table 2). The Antarctic plate is expected to be near stationary, because it is almost entirely surrounded by spreading ridges that leads to a unique geometry of boundary forces. There is, however, a short subduction zone south of the Chile Ridge, where the Antarctic plate subducts underneath South America. The fact that GSRM-APM-1 predicts Antarctic motion toward this subduction zone (Figure 5), may suggest that the slab-pull force there is responsible for the plate's motion, similar to the mechanism for fast-moving plates. GSRM-APM-1 confirms recent arguments [*Hamilton*, 2003, 2007] that most geodynamical processes (e.g., subduction hinge roll-back, plate motion toward subduction zones, migrating ridges) are best explained when $\vec{v}_{APM}$ is approximated by a fixed Antarctic plate reference frame. *Schellart et al.* [2008] confirmed that the number of retreating trenches is largest in an Antarctic-fixed reference frame, but discarded the appropriateness of this frame because it does not well in minimizing trench migration velocities and toroidal mantle flux caused by slab migration. Although close to an Antarctic-fixed reference frame, GSRM-APM-1 is different from any of the frames tested by *Schellart et al.* [2008] (as well as by *Funiciello et al.* [2008] and *Lallemand et al.* [2008]) and further study is required to test GSRM-APM-1 in light of expected subduction dynamics.

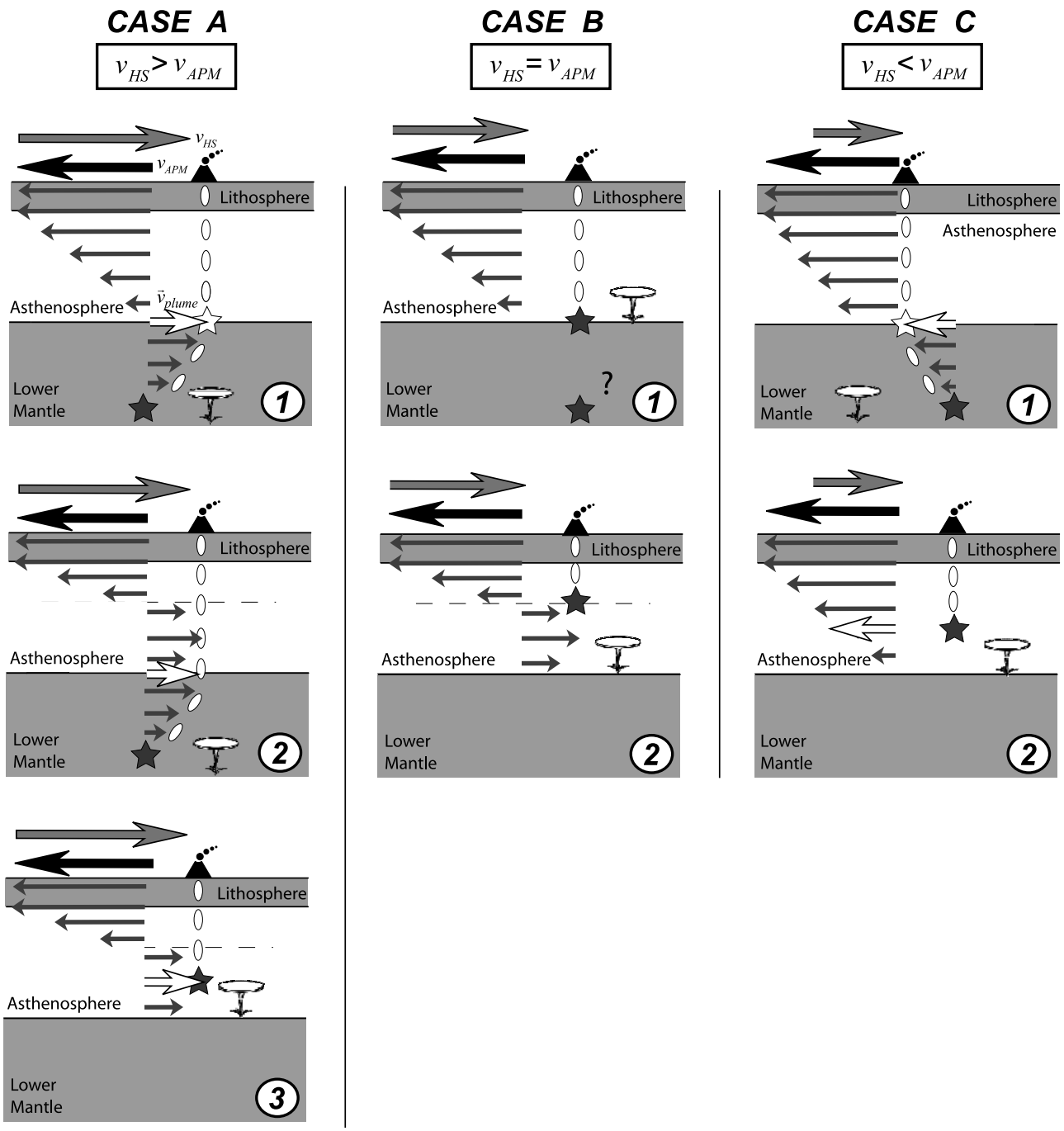

Figure 9. Illustration of simple cases that can explain inferred plume motions $\vec{v}_{plume}$ in terms of asthenospheric or subasthenospheric flow depending on the depth origin of the plume. Cases are divided as $v_{HS} > v_{APM}$ (case A), $v_{HS} = v_{APM}$ (within uncertainty) (case B), or $v_{HS} < v_{APM}$ (case C). Black arrow is $\vec{v}_{APM}$, gray arrow is $\vec{v}_{HS}$, and white vector is $\vec{v}_{plume}$. The latter is interpreted as the velocity of a plume (white ellipses) relative to a point at or below the base of asthenosphere (thumbnail). Open star is plume location after deviation from original position (black star) due to subasthenospheric flow. For simplicity the cases considered are restricted to 2-D flow, and $\vec{v}_{APM}$ and $\vec{v}_{HS}$ are assumed to be antiparallel. It is assumed that although simple asthenospheric shear flow may deflect a plume (not shown), it does not alter the horizontal plume velocity acquired at depth [e.g., *Steinberger*, 2000; *Steinberger et al.*, 2004]. Cases are discussed in the text and examples are given.

7.3. Net Rotation

[49] The net rotation of GSRM-APM-1 is 0.2065°/Ma counterclockwise around a pole in the southern Indian Ocean, corresponding to a maximum velocity of 23.0 mm/a. The rotation rate is 47% of HS3-NUVEL1A. *Becker* [2008] concluded that ~50% of HS3-NUVEL1A is required to match global azimuthal anisotropy observations with mantle flow models that include strong continental keels. The

consistency between my result and Becker's suggests that my approach can validly constrain the lithosphere's net rotation, even when no mantle flow is considered (other than the asthenospheric simple shear flow that accommodates lithosphere-mesosphere differential motion).

[50] Studies that consider both density-driven and plate-driven flow find that an asthenospheric viscosity of about $3.5-5 \times 10^{19}$ Pa s is required to match φ_{SKS} observations [*Behn et al.*, 2004; *Conrad et al.*, 2007]. I therefore argue that these viscosity levels (which are constrained to be 0.1 times that of the upper mantle) are needed to match the rate of net rotation reported here (i.e., 0.2065°/Ma). Asthenospheric viscosity levels of $3.5-5 \times 10^{19}$ Pa s are very near those found, for example, to match postglacial uplift observations [e.g., *Cathles*, 1975; *Fjeldskaar*, 1994].

[51] It is important to emphasize that the net rotation discussed here does not imply that all of the Earth's surface moves westward, as was originally advocated by *Doglioni* [1990]. Not only would the net rotation of such a model (1.4901°/Ma [*Cuffaro and Doglioni*, 2007]) imply a very large misfit with the global φ_{SKS} database, the required viscosity ($\sim 5 \times 10^{17}$ Pa s [e.g., *Doglioni et al.*, 2005; *Scoppola et al.*, 2006]) would have to be 2–3 orders of magnitude lower than the typical values reported above. Moreover, to match $\vec{v}_{HS}$ observations, a model of very fast net rotation requires hot spot plumes to originate in the midasthenosphere (with simple channel flow). A good portion of hot spot plumes originate, however, below the asthenosphere [e.g., *Courtillot et al.*, 2003; *Montelli et al.*, 2006; *Boschi et al.*, 2007; *Zhao*, 2007].

7.4. Mantle Flow and Plate Driving Forces

[52] I obtain estimates of asthenospheric and subasthenospheric mantle flow by combining GSRM-APM-1 plate motion predictions, hot spot propagation vectors, new depth estimates of plume sources, and constraints on mantle flow from dynamical models. Through this combination, the hot spots are essentially used as piercing points to image mantle flow.

[53] A consistent picture appears for mantle flow underneath oceans. Far away (>1000 km) from ridges and subduction zones, simple asthenospheric shear flow persists, with subasthenospheric flow velocities relatively small and roughly antiparallel to $\vec{v}_{APM}$. This counterflow is predicted for fast-moving plates when plate motion is decoupled from the mesosphere by a low-viscosity asthenosphere [*Hager and O'Connell*, 1979]. The counterflow beneath Hawaii is fairly oblique to plate motions and may indicate that lower-mantle flow is actually controlled by density flow toward the large mantle upwelling in the southern Pacific. My results indicate that asthenospheric return flow exists underneath oceanic lithosphere within <1000 km of spreading ridges, and that the return flow velocity is of equal magnitude to the surface motion. An additional counterflow component in the subasthenospheric mantle may be present as well.

[54] The lack of continental hot spots with deep plumes prevents me from placing direct constraints on the subasthenospheric flow field underneath continents. Nevertheless, some inferences on the plate driving forces for continents can still be made when combining my results with other studies' conclusions on the mantle flow field and the characteristics of the GSRM-APM-1 velocity field. The fastest moving continent is Australia. The Australian plate has a relatively large portion of oceanic lithosphere and a long significant subduction zone controlling its fast northward motion. The continent-oceanic make-up of the Nubian plate is quite similar to Australia except that active subduction of Nubia underneath Eurasia is limited to the short Hellenic trench, explaining Nubia's relatively slow present-day motion. The westward motion of South and North America at ~2 cm/a cannot solely be controlled by slab pull along short subduction segments in the Caribbean. The question of which other forces drive these plates has been much debated [e.g., *Stefanick and Jurdy*, 1992; *Bokelmann*, 2002b; *Liu and Bird*, 2002; *Humphreys and Coblentz*, 2007]. The results reported here support asthenospheric counterflow in western North America. The origin of this flow field must be found in the eastward flow of the mesosphere [*Steinberger*, 2000; *Silver and Holt*, 2002; *Becker et al.*, 2006; *Moucha et al.*, 2008], which opposes plate motion and requires a complete decoupling in the asthenosphere. It has been proposed that this eastward flow (at ~2–3 cm/a) is induced by the downwelling of the old Farallon slab underneath eastern North America [e.g., *Becker et al.*, 2006; *Forte et al.*, 2007]. An opposite westward flow of ~2 cm/a is predicted east of this downwelling [*Conrad et al.*, 2004; *Forte et al.*, 2007], very close in direction and speed to the plate motion estimate of GSRM-APM-1. The motion of North America can thus be explained through mantle flow below (north-) eastern North America at APM speed (or probably slightly higher), that is strongly coupled to the lithosphere. *Bokelmann* [2002a, 2002b] arrived at a similar driving mechanism scenario based on the westward dip direction of fast seismic orientations in (north-) eastern North America (as opposed to eastward dipping fast axes in western North America). In this dynamic model, the mantle would be leading the lithosphere in eastern North America. Unfortunately there is no recent hot spot track there associated with a deep plume to confirm this. However, a correlation analysis between the locations of Cretaceous igneous rocks in New England with a low-velocity anomaly in the craton beneath the Great Lakes (proposed to be caused by the Great Meteor hot spot plume) suggested ~ 4 mm/a of westward motion of the bottom of the lithosphere relative to the surface [*Eaton and Frederiksen*, 2007]. These findings could most simply be explained by mantle flow that is strongly coupled to the lithosphere and moving only slightly faster than the surface. *Liu and Bird* [2002] found that surface kinematics and stress observations can be explained when the mantle leads the lithosphere up to 3 mm/a.

[55] Westward forward drag is thought to be the main driving force of the North American plate (as well as other plates) [e.g., *Bird*, 1998; *Bird et al.*, 2008; *Lithgow-Bertelloni and Guynn*, 2004; *Ghosh et al.*, 2008]. However, this process can only occur for the eastern part of the continent, because of the inferred mantle-lithosphere decoupling in western North America. In western North America, the deformation must therefore be controlled by plate boundary and lithospheric buoyancy forces [e.g., *Flesch et al.*, 2000, 2007; *Humphreys and Coblentz*, 2007]. Moreover, the decoupling in western North America explains why no vertically coherent deformation between mantle and litho-

sphere is observed [e.g., *Savage and Sheehan*, 2000]. The North American plate may be a good example of how mantle density anomalies (other than those associated with attached slabs) can drive continental plates through convection-controlled forward basal drag. No such an anomaly is present underneath a plate like Eurasia, which as a result is nearly stationary.

8. Conclusions

[56] Velocities in the GSRM-APM-1 frame at every 0.5° for the entire Earth's surface can be found here: http://earthref.org/cgi-bin/er.cgi?s=erda.cgi?n=972. GSRM-APM-1 may be the first APM model to provide a self-consistent framework for explaining relative surface motions, mantle anisotropy, and hot spot motions in the context of mantle dynamics. This conclusion is confirmed by the pattern of surface motions away from ridges and toward trenches in GSRM-APM-1 (even for slow plates). Moreover, I find that GSRM-APM-1's prediction of lithospheric net rotation relative to the mesosphere is consistent with the expected net rotation in recent studies that considered mantle flow.

[57] I find that observed anisotropy orientations are to first order controlled by plate motions, as supported by φ_{SKS} observations which fit equally well for most cratons and oceans. Effects from mantle flow and lithospheric anisotropy on φ_{SKS} can be considered minor on a global scale. Most of the φ_{SKS} values used in this study are based on the assumption that anisotropy originates in a single layer. APM models based on φ_{SKS} could be improved when future φ_{SKS} estimates are more conclusively ascribed to asthenospheric anisotropy alone. This may soon be possible due to the mounting evidence that different lithospheric and asthenospheric anisotropy can be identified, and that asthenospheric anisotropy aligns to φ_{APM}. However, given the robustness of GSRM-APM-1, future APM models based on φ_{SKS} observations may not change much. Instead, φ_{APM} estimates from GSRM-APM-1 may be used as an aid in separating observed seismic anisotropy parameters into the proper asthenospheric and lithospheric contributions. Once splitting parameters can be uniquely related to asthenospheric anisotropy, a comparison between splitting delay times, ds, and v_{APM} may yield new insight into shear-induced LPO. With the current database of splitting parameters, I find no correlation between ds and v_{APM}.

[58] **Acknowledgments.** I thank J. Hammond, A. Reading, and F. Fontaine for providing additional data needed to include their results in the φ_{SKS} compilation. I thank G. Blewitt, W. Holt, and P. Silver for discussions, two anonymous reviewers for comments on an earlier manuscript draft, G. Bokelmann and an anonymous reviewer for comments on the final manuscript, and R. Penfield for significantly improving the clarity of the paper. Figures 1, 2, 5, 6, and 8 were made with Generic Mapping Tools (v. 4.2) [*Wessel and Smith*, 1991].

References

Argus, D. F., and R. G. Gordon (1991), No-net rotation model of current plate velocities incorporating plate motion model NUVEL-1, *Geophys. Res. Lett.*, *18*, 2039–2042, doi:10.1029/91GL01532.

Artemieva, I. M., and W. D. Mooney (2002), On the relations between cratonic lithosphere thickness, plate motions, and basal drag, *Tectonophysics*, *358*, 211–231, doi:10.1016/S0040-1951(02)00425-0.

Assumpção, M., M. Heintz, A. Vauchez, and M. E. Silva (2006), Upper mantle anisotropy in SE and central Brazil from SKS splitting: Evidence of asthenospheric flow around a cratonic keel, *Earth Planet. Sci. Lett.*, *250*, 224–240, doi:10.1016/j.epsl.2006.07.038.

Bank, C., M. Bostock, R. Ellis, and J. Cassidy (2000), A reconnaissance teleseismic study of the upper mantle and transition zone beneath the Archean Slave craton in NW Canada, *Tectonophysics*, *319*, 151–166, doi:10.1016/S0040-1951(00)00034-2.

Barruol, G., and W. Ben Ismail (2001), Upper mantle anisotropy beneath the African IRIS and Geoscope stations, *Geophys. J. Int.*, *146*, 549–561, doi:10.1046/j.0956-540x.2001.01481.x.

Barruol, G., and R. Hoffmann (1999), Upper mantle anisotropy beneath the Geoscope stations, *J. Geophys. Res.*, *104*, 10,757–10,773, doi:10.1029/1999JB900033.

Becker, T. W. (2006), On the effect of temperature and strain-rate dependent viscosity on global mantle flow, net rotation, and plate-driving forces, *Geophys. J. Int.*, *167*, 943–957, doi:10.1111/j.1365-246X.2006.03172.x.

Becker, T. W. (2008), Azimuthal seismic anisotropy constrains net rotation of the lithosphere, *Geophys. Res. Lett.*, *35*, L05303, doi:10.1029/2007GL032928.

Becker, T. W., J. B. Kellogg, G. Ekström, and R. J. O'Connell (2003), Comparison of azimuthal seismic anisotropy from surface waves and finite strain from global mantle-circulation models, *Geophys. J. Int.*, *155*, 696–714, doi:10.1046/j.1365-246X.2003.02085.x.

Becker, T. W., V. Schulte-Pelkum, D. K. Blackman, J. B. Kellogg, and R. J. O'Connell (2006), Mantle flow under the western United States from shear wave splitting, *Earth Planet. Sci. Lett.*, *247*, 235–251, doi:10.1016/j.epsl.2006.05.010.

Becker, T. W., G. Ekström, L. Boschi, and J. H. Woodhouse (2007), Length scales, patterns and origin of azimuthal seismic anisotropy in the upper mantle as mapped by Rayleigh waves, *Geophys. J. Int.*, *171*, 451–462, doi:10.1111/j.1365-246X.2007.03536.x.

Behn, M. D., C. P. Conrad, and P. G. Silver (2004), Detection of upper mantle flow associated with the African Superplume, *Earth Planet. Sci. Lett.*, *224*, 259–274, doi:10.1016/j.epsl.2004.05.026.

Bird, P. (1998), Testing hypotheses on plate-driving mechanisms with global lithosphere models including topography, thermal structure, and faults, *J. Geophys. Res.*, *103*, 10,115–10,129, doi:10.1029/98JB00198.

Bird, P., Z. Liu, and W. K. Rucker (2008), Stresses that drive the plates from below: Definitions, computational path, model optimization, and error analysis, *J. Geophys. Res.*, *113*, B11406, doi:10.1029/2007JB005460.

Blackman, D. K., and J. Kendall (2002), Seismic anisotropy in the upper mantle 2. Predictions for current plate boundary flow models, *Geochem. Geophys. Geosyst.*, *3*(9), 8602, doi:10.1029/2001GC000247.

Bokelmann, G. H. R. (2002a), Which forces drive North America?, *Geology*, *30*, 1027–1030, doi:10.1130/0091-7613(2002)030<1027:WFDNA>2.0.CO;2.

Bokelmann, G. H. R. (2002b), Convection-driven motion of the North American craton: Evidence from *P* wave anisotropy, *Geophys. J. Int.*, *148*, 278–287, doi:10.1046/j.1365-246X.2002.01614.x.

Boschi, L., T. W. Becker, and B. Steinberger (2007), Mantle plumes: Dynamic models and seismic images, *Geochem. Geophys. Geosyst.*, *8*, Q10006, doi:10.1029/2007GC001733.

Burke, K., and J. T. Wilson (1972), Is the African plate stationary?, *Nature*, *239*, 387–390, doi:10.1038/239387b0.

Cathles, L. M. (1975), *The Viscosity of the Earth's Mantle*, Princeton Univ. Press, Princeton, N. J.

Christiansen, R. L., G. R. Foulger, and J. R. Evans (2002), Upper-mantle origin of the Yellowstone hotspot, *Geol. Soc. Am. Bull.*, *114*, 1245–1256, doi:10.1130/0016-7606(2002)114<1245:UMOOTY>2.0.CO;2.

Clitheroe, G., and R. van der Hilst (1998), Complex anisotropy in the Australian lithosphere from shear-wave splitting in broad-band SKS records, in *Structure and Evolution of the Australian Continent*, vol. 26, edited by J. Braun et al., pp. 73–78, AGU, Washington, D. C.

Conrad, C. P., C. Lithgow-Bertelloni, and K. E. Louden (2004), Iceland, the Farallon slab, and dynamic topography of the North Atlantic, *Geology*, *32*, 177–180, doi:10.1130/G20137.1.

Conrad, C. P., M. D. Behn, and P. G. Silver (2007), Global mantle flow and the development of seismic anisotropy: Differences between the oceanic and continental upper mantle, *J. Geophys. Res.*, *112*, B07317, doi:10.1029/2006JB004608.

Courtillot, V., A. Davaille, J. Besse, and J. Stock (2003), Three distinct types of hotspots in the Earth's mantle, *Earth Planet. Sci. Lett.*, *205*, 295–308, doi:10.1016/S0012-821X(02)01048-8.

Cuffaro, M., and C. Doglioni (2007), Global kinematics in deep versus shallow hotspot reference frames, in *Plates, Plumes, and Planetary Processes*, vol. 430, edited by G. R. Foulger and D. M. Jurdy, pp. 359–374, Geol. Soc. of Am., Boulder, Colo.

Debayle, E., B. Kennett, and K. Priestley (2005), Global azimuthal seismic anisotropy and the unique plate-motion deformation of Australia, *Nature*, *433*, 509–512, doi:10.1038/nature03247.

DeMets, C., R. G. Gordon, D. F. Argus, and S. Stein (1994), Effect of recent revisions to the geomagnetic reversal time-scale on estimates of current plate motions, *Geophys. Res. Lett.*, *21*, 2191–2194, doi:10.1029/94GL02118.

Deschamps, F., S. Lebedev, T. Meier, and J. Trampert (2008), Stratified seismic anisotropy reveals past and present deformation beneath the east-central United States, *Earth Planet. Sci. Lett.*, *274*, 489–498, doi:10.1016/j.epsl.2008.07.058.

DiVenere, V., and D. V. Kent (1999), Are the Pacific and Indo-Atlantic hotspots fixed? Testing the plate circuit through Antarctica, *Earth Planet. Sci. Lett.*, *170*, 105–117, doi:10.1016/S0012-821X(99)00096-5.

Doglioni, C. (1990), The global tectonic pattern, *J. Geodyn.*, *12*, 21–38, doi:10.1016/0264-3707(90)90022-M.

Doglioni, C., D. Green, and F. Mongelli (2005), On the shallow origin of hotspots and the westward drift of the lithosphere, in *Plates, Plumes, and Paradigms*, vol. 388, edited by G. R. Foulger et al., pp. 735–749, Geol. Soc. of Am., Boulder, Colo.

Eaton, D., A. Frederiksen, and S. Miong (2004), Shear-wave splitting observations in the lower Great Lakes region: Evidence for regional anisotropic domains and keel-modified asthenospheric flow, *Geophys. Res. Lett.*, *31*, L07610, doi:10.1029/2004GL019438.

Eaton, D. W., and A. Frederiksen (2007), Seismic evidence for convection-driven motion of the North American plate, *Nature*, *446*(7134), 428–431, doi:10.1038/nature05675.

Evans, M. S., J. Kendall, and R. J. Willemann (2006), Automated SKS splitting and upper-mantle anisotropy beneath Canadian seismic stations, *Geophys. J. Int.*, *165*, 931–942, doi:10.1111/j.1365-246X.2006.02973.x.

Fjeldskaar, W. (1994), Viscosity and thickness of the asthenosphere detected from the Fennoscandian uplift, *Earth Planet. Sci. Lett.*, *126*, 399–410, doi:10.1016/0012-821X(94)90120-1.

Flesch, L. M., W. E. Holt, A. J. Haines, and B. Shen-Tu (2000), Dynamics of the Pacific-North American plate boundary in the western United States, *Science*, *287*, 834–836, doi:10.1126/science.287.5454.834.

Flesch, L. M., W. E. Holt, A. J. Haines, L. X. Wen, and B. Shen-Tu (2007), The dynamics of western North America: Stress magnitudes and the relative role of gravitational potential energy, plate interaction at the boundary and basal tractions, *Geophys. J. Int.*, *169*, 866–896, doi:10.1111/j.1365-246X.2007.03274.x.

Fontaine, F. R., G. Barruol, A. Tommasi, and G. Bokelmann (2007), Upper-mantle flow beneath French Polynesia from shear wave splitting, *Geophys. J. Int.*, *170*, 1262–1288, doi:10.1111/j.1365-246X.2007.03475.x.

Forsyth, D., and S. Uyeda (1975), On the relative importance of the driving forces of plate motion, *Geophys. J. R. Astron. Soc.*, *43*, 163–200.

Forte, A. M., and J. X. Mitrovica (2001), Deep-mantle high-viscosity flow and thermochemical structure inferred from seismic and geodynamic data, *Nature*, *410*, 1049–1056, doi:10.1038/35074000.

Forte, A. M., J. X. Mitrovica, R. Moucha, N. A. Simmons, and S. P. Grand (2007), Descent of the ancient Farallon slab drives localized mantle flow below the New Madrid seismic zone, *Geophys. Res. Lett.*, *34*, L04308, doi:10.1029/2006GL027895.

Fouch, M. J., and S. Rondenay (2006), Seismic anisotropy beneath stable continental interiors, *Phys. Earth Planet. Inter.*, *158*, 292–320, doi:10.1016/j.pepi.2006.03.024.

Fouch, M. J., K. M. Fischer, E. M. Parmentier, M. E. Wysession, and T. J. Clarke (2000), Shear wave splitting, continental keels, and patterns of mantle flow, *J. Geophys. Res.*, *105*, 6255–6275, doi:10.1029/1999JB900372.

Frederiksen, A. W., I. J. Ferguson, D. Eaton, S.-K. Miong, and E. Gowan (2006), Mantle fabric at multiple scales across an Archean-Proterozoic boundary, Grenville Front, Canada, *Phys. Earth Planet. Inter.*, *158*, 240–263, doi:10.1016/j.pepi.2006.03.025.

Funiciello, F., C. Faccenna, A. Heuret, S. Lallemand, E. Di Giuseppe, and T. Becker (2008), Trench migration, net rotation and slab-mantle coupling, *Earth Planet. Sci. Lett.*, *271*, 233–240, doi:10.1016/j.epsl.2008.04.006.

Gaboret, C., A. Forte, and J. Montagner (2003), The unique dynamics of the Pacific hemisphere mantle and its signature on seismic anisotropy, *Earth Planet. Sci. Lett.*, *208*, 219–233, doi:10.1016/S0012-821X(03)00037-2.

Gao, S. S., K. H. Liu, R. J. Stern, G. R. Keller, J. P. Hogan, J. Pulliam, and E. Y. Anthony (2008), Characteristics of mantle fabrics beneath the south-central United States: Constraints from shear-wave splitting measurements, *Geosphere*, *4*, 411–417, doi:10.1130/GES00159.1.

Ghosh, A., W. E. Holt, L. Wen, A. J. Haines, and L. M. Flesch (2008), Joint modeling of lithosphere and mantle dynamics elucidating lithosphere-mantle coupling, *Geophys. Res. Lett.*, *35*, L16309, doi:10.1029/2008GL034365.

Gordon, R. G., and D. M. Jurdy (1986), Cenozoic global plate motions, *J. Geophys. Res.*, *91*, 12,389–12,406, doi:10.1029/JB091iB12p12389.

Gordon, R. G., A. Cox, and C. E. Harter (1978), Absolute motion of an individual plate estimated from its ridge and trench boundaries, *Nature*, *274*, 752–755, doi:10.1038/274752a0.

Gripp, A. E., and R. G. Gordon (2002), Young tracks of hotspots and current plate velocities, *Geophys. J. Int.*, *150*, 321–361, doi:10.1046/j.1365-246X.2002.01627.x.

Gung, Y., M. Panning, and B. Romanowicz (2003), Global anisotropy and the thickness of continents, *Nature*, *422*, 707–711, doi:10.1038/nature01559.

Hager, B. H., and R. J. O'Connell (1979), Kinematic models of large-scale flow in the Earth's mantle, *J. Geophys. Res.*, *84*, 1031–1048, doi:10.1029/JB084iB03p01031.

Hamilton, W. B. (2003), An alternative Earth, *GSA Today*, *13*, 4–12, doi:10.1130/1052-5173(2003)013<0004:AAE>2.0.CO;2.

Hamilton, W. B. (2007), Driving mechanism and 3-D circulation of plate tectonics, in *Whence the Mountains? Inquiries into the Evolution of Orogenic Systems: A Volume in Honor of Raymond A. Price*, vol. 433, edited by J. W. Sears, T. A. Harms, and C. A. Evenchick1–25, doi:10.1130/2007.2433(01), Geol. Soc. of Am., Boulder, Colo.

Hansen, S., S. Schwartz, A. Al-Amri, and A. Rodgers (2006), Combined plate motion and density-driven flow in the asthenosphere beneath Saudi Arabia: Evidence from shear-wave splitting and seismic anisotropy, *Geology*, *34*, 869–872, doi:10.1130/G22713.1.

Harmon, N., D. W. Forsyth, K. M. Fischer, and S. C. Webb (2004), Variations in shear-wave splitting in young Pacific seafloor, *Geophys. Res. Lett.*, *31*, L15609, doi:10.1029/2004GL020495.

Harper, J. F. (1975), On the driving forces of plate tectonics, *Geophys. J. Int.*, *40*, 465–474, doi:10.1111/j.1365-246X.1975.tb04143.x.

Heintz, M., and B. L. Kennett (2005), Continental scale shear wave splitting analysis: Investigation of seismic anisotropy underneath the Australian continent, *Earth Planet. Sci. Lett.*, *236*, 106–119, doi:10.1016/j.epsl.2005.05.003.

Heintz, M., A. Vauchez, M. Assumpção, G. Barruol, and M. Egydio-Silva (2003), Shear wave splitting in SE Brazil: An effect of active or fossil upper mantle flow, or both?, *Earth Planet. Sci. Lett.*, *211*, 79–95, doi:10.1016/S0012-821X(03)00163-8.

Hooft, E. E., D. R. Toomey, and S. C. Solomon (2003), Anomalously thin transition zone beneath the Galápagos hotspot, *Earth Planet. Sci. Lett.*, *216*, 55–64, doi:10.1016/S0012-821X(03)00517-X.

Humphreys, E. D., and D. D. Coblentz (2007), North America dynamics and western U.S. tectonics, *Rev. Geophys.*, *45*, RG3001, doi:10.1029/2005RG000181.

Illies, J., C. Prodehl, H. Schmincke, and A. Semmel (1979), The quaternary uplift of the rhenish shield in Germany, *Tectonophysics*, *61*(1–3), 197–225, doi:10.1016/0040-1951(79)90298-1.

Kaminski, É., and N. M. Ribe (2002), Timescales for the evolution of seismic anisotropy in mantle flow, *Geochem. Geophys. Geosyst.*, *3*(8), 1051, doi:10.1029/2001GC000222.

Kaula, W. (1975), Absolute plate motions by boundary velocity minimizations, *J. Geophys. Res.*, *80*, 244–248, doi:10.1029/JB080i002p00244.

Kay, I., S. Sol, J.-M. Kendall, C. Thomson, D. White, I. Asudeh, B. Roberts, and D. Francis (1999), Shear wave splitting observations in the Archean Craton of western Superior, *Geophys. Res. Lett.*, *26*(17), 2669–2672, doi:10.1029/1999GL010493.

Kendrick, E., M. Bevis, R. Smalley, B. Brooks, R. B. Vargas, E. Lauría, and L. P. S. Fortes (2003), The Nazca-South America Euler vector and its rate of change, *J. South Am. Earth Sci.*, *16*, 125–131, doi:10.1016/S0895-9811(03)00028-2.

Klosko, E. R., R. M. Russo, E. A. Okal, and W. P. Richardson (2001), Evidence for a rheologically strong chemical mantle root beneath the Ontong-Java Plateau, *Earth Planet. Sci. Lett.*, *186*, 347–361, doi:10.1016/S0012-821X(01)00235-7.

Koppers, A. A. P., J. P. Morgan, J. W. Morgan, and H. Staudigel (2001), Testing the fixed hotspot hypothesis using $^{40}Ar/^{39}Ar$ age progressions along seamount trails, *Earth Planet. Sci. Lett.*, *185*, 237–252, doi:10.1016/S0012-821X(00)00387-3.

Kreemer, C., and W. E. Holt (2001), A no-net rotation model of present-day surface motions, *Geophys. Res. Lett.*, *28*, 4407–4410, doi:10.1029/2001GL013232.

Kreemer, C., W. E. Holt, and A. J. Haines (2003), An integrated global model of present-day plate motions and plate boundary deformation, *Geophys. J. Int.*, *154*, 8–34, doi:10.1046/j.1365-246X.2003.01917.x.

Kreemer, C., D. Lavallée, G. Blewitt, and W. E. Holt (2006), On the stability of a geodetic no-net rotation frame and its implication for the International Terrestrial Reference Frame, *Geophys. Res. Lett.*, *33*, L17306, doi:10.1029/2006GL027058.

Kreemer, C., G. Blewitt, W. C. Hammond, and R. A. Bennett (2008), Geodetic constraints on strain transfer between the Colorado Plateau and the Basin and Range Province, *Eos Trans. AGU*, *89*(53), Fall Meet. Suppl., Abstract G34A–06.

Kubo, A., and Y. Hiramatsu (1998), On presence of seismic anisotropy in the asthenosphere beneath continents and its dependence on plate velocity: Significance of reference frame selection, *Pure Appl. Geophys.*, *151*, 281–303, doi:10.1007/s000240050115.

Kumar, M. R., and A. Singh (2008), Evidence for plate motion related strain in the Indian shield from shear wave splitting measurements, *J. Geophys. Res.*, *113*, B08306, doi:10.1029/2007JB005128.

Lallemand, S., A. Heuret, C. Faccenna, and F. Funiciello (2008), Subduction dynamics as revealed by trench migration, *Tectonics*, *27*, TC3014, doi:10.1029/2007TC002212.

Le Pichon, X. (1968), Sea-floor spreading and continental drift, *J. Geophys. Res.*, *73*, 3661–3697, doi:10.1029/JB073i012p03661.

Lévêque, J. J., E. Debayle, and V. Maupin (1998), Anisotropy in the Indian Ocean upper mantle from Rayleigh- and Love-waveform inversion, *Geophys. J. Int.*, *133*, 529–540, doi:10.1046/j.1365-246X.1998.00504.x.

Levin, V., W. Menke, and J. Park (2000), No regional anisotropic domains in the northeastern U.S. Appalachians, *J. Geophys. Res.*, *105*, 19,029–19,042, doi:10.1029/2000JB900123.

Lithgow-Bertelloni, C., and J. H. Guynn (2004), Origin of the lithospheric stress field, *J. Geophys. Res.*, *109*, B01408, doi:10.1029/2003JB002467.

Liu, Z., and P. Bird (2002), North America plate is driven westward by lower mantle flow, *Geophys. Res. Lett.*, *29*(24), 2164, doi:10.1029/2002GL016002.

Lliboutry, L. (1974), Plate motion relative to rigid lower mantle, *Nature*, *250*, 298–300, doi:10.1038/250298a0.

Long, M. D., and P. G. Silver (2008), The subduction zone flow field from seismic anisotropy: A global view, *Science*, *319*, 315–318, doi:10.1126/science.1150809.

Long, M. D., and P. G. Silver (2009), Mantle flow in subduction systems: Subslab flow field and implications for mantle dynamics, *J. Geophys. Res.*, doi:10.1029/2008JB006200, in press.

Maggi, A., E. Debayle, K. Priestley, and G. Barruol (2006), Azimuthal anisotropy of the Pacific region, *Earth Planet. Sci. Lett.*, *250*, 53–71, doi:10.1016/j.epsl.2006.07.010.

Marks, K. M., and J. M. Stock (1994), Variations in ridge morphology and depth-age relationships on the Pacific-Antarctic ridge, *J. Geophys. Res.*, *99*, 531–541, doi:10.1029/93JB02760.

Marone, F., and B. Romanowicz (2007), The depth distribution of azimuthal anisotropy in the continental upper mantle, *Nature*, *447*, 198–201, doi:10.1038/nature05742.

Marquart, G., H. Schmeling, and O. Čadek (2007), Dynamic models for mantle flow and seismic anisotropy in the North Atlantic region and comparison with observations, *Geochem. Geophys. Geosyst.*, *8*, Q02008, doi:10.1029/2006GC001359.

Merkouriev, S., and C. DeMets (2006), Constraints on Indian plate motion since 20 Ma from dense Russian magnetic data: Implications for Indian plate dynamics, *Geochem. Geophys. Geosyst.*, *7*, Q02002, doi:10.1029/2005GC001079.

Minster, B. J., and T. H. Jordan (1978), Present-day plate motions, *J. Geophys. Res.*, *83*, 5331–5354, doi:10.1029/JB083iB11p05331.

Molnar, P., and J. Stock (1987), Relative motions of hotspots in the Pacific, Atlantic and Indian Oceans since late Cretaceous time, *Nature*, *327*, 587–591, doi:10.1038/327587a0.

Montagner, J., and T. Tanimoto (1991), Global upper mantle tomography of seismic velocities and anisotropies, *J. Geophys. Res.*, *96*, 20,337–20,351, doi:10.1029/91JB01890.

Montelli, R., G. Nolet, F. A. Dahlen, and G. Masters (2006), A catalogue of deep mantle plumes: New results from finite-frequency tomography, *Geochem. Geophys. Geosyst.*, *7*, Q11007, doi:10.1029/2006GC001248.

Morgan, W. J. (1971), Convection plumes in the lower mantle, *Nature*, *230*, 42–43, doi:10.1038/230042a0.

Morgan, W. J., and J. Phipps Morgan (2007), Plate velocities in the hotspot reference frame, in *Plates, Plumes, and Planetary Processes*, vol. 430, edited by G. R. Foulger and D. M. Jurdy, pp. 65–78, Geol. Soc. of Am., Boulder, Colo.

Moucha, R., A. M. Forte, D. B. Rowley, J. X. Mitrovica, N. A. Simmons, and S. P. Grand (2008), Mantle convection and the recent evolution of the Colorado Plateau and the Rio Grande Rift valley, *Geology*, *36*, 439–442, doi:10.1130/G24577A.1.

Müller, R., J. Y. Royer, and L. A. Lawver (1993), Revised plate motions relative to the hotspots from combined Atlantic and Indian Ocean hotspot tracks, *Geology*, *21*, 275–278, doi:10.1130/0091-7613(1993)021<0275:RPMRTT>2.3.CO;2.

O'Connell, R., C. Gable, and B. Hager (1991), Toroidal-poloidal partitioning of lithospheric plate motions, in *NATO Advanced Research Workshop Glacial Isostasy: Sea-Level and Mantle Rheology*, edited by R. Sabadini, K. Lambeck, and E. Boschi, pp. 535–551, Kluwer Acad., Dordrecht, Netherlands.

O'Neill, C., D. Müller, and B. Steinberger (2003), Geodynamic implications of moving Indian Ocean hotspots, *Earth Planet. Sci. Lett.*, *215*, 151–168, doi:10.1016/S0012-821X(03)00368-6.

O'Neill, C., D. Müller, and B. Steinberger (2005), On the uncertainties in hot spot reconstructions and the significance of moving hot spot reference frames, *Geochem. Geophys. Geosyst.*, *6*, Q04003, doi:10.1029/2004GC000784.

Park, J., and V. Levin (2002), Seismic anisotropy: Tracing plate dynamics in the mantle, *Science*, *296*, 485–489, doi:10.1126/science.1067319.

Pilidou, S., K. Priestley, E. Debayle, and Ó. Gudmundsson (2005), Rayleigh wave tomography in the North Atlantic: High resolution images of the Iceland, Azores and Eifel mantle plumes, *Lithos*, *79*, 453–474, doi:10.1016/j.lithos.2004.09.012.

Podolefsky, N. S., S. Zhong, and A. K. McNamara (2004), The anisotropic and rheological structure of the oceanic upper mantle from a simple model of plate shear, *Geophys. J. Int.*, *158*, 287–296, doi:10.1111/j.1365-246X.2004.02250.x.

Press, W. H., S. A. Teukolsky, W. T. Vetterling, and B. P. Flannery (1992), *Numerical Recipes in Fortran 77*, Cambridge Univ. Press, New York.

Reading, A. M., and M. Heintz (2008), Seismic anisotropy of east Antarctica from shear-wave splitting: Spatially varying contributions from lithospheric structural fabric and mantle flow?, *Earth Planet. Sci. Lett.*, *268*, 433–443, doi:10.1016/j.epsl.2008.01.041.

Ricard, Y., C. Doglioni, and R. Sabadini (1991), Differential rotation between lithosphere and mantle: A consequence of lateral mantle viscosity variations, *J. Geophys. Res.*, *96*, 8407–8415, doi:10.1029/91JB00204.

Ritter, J. R., M. Jordan, U. R. Christensen, and U. Achauer (2001), A mantle plume below the Eifel volcanic fields, Germany, *Earth Planet. Sci. Lett.*, *186*, 7–14, doi:10.1016/S0012-821X(01)00226-6.

Ritzwoller, M. H., N. M. Shapiro, A. L. Levshin, and G. M. Leahy (2001), Crustal and upper mantle structure beneath Antarctica and surrounding oceans, *J. Geophys. Res.*, *106*, 30,645–30,670, doi:10.1029/2001JB000179.

Russo, R. M., and E. A. Okal (1998), Shear wave splitting and upper mantle deformation in French Polynesia: Evidence for small-scale heterogeneity related to the Society hotspot, *J. Geophys. Res.*, *103*, 15,089–15,108, doi:10.1029/98JB01075.

Savage, M. K. (1999), Seismic anisotropy and mantle deformation: What have we learned from shear wave splitting?, *Rev. Geophys.*, *37*, 65–106, doi:10.1029/98RG02075.

Savage, M. K., and A. F. Sheehan (2000), Seismic anisotropy and mantle flow from the Great Basin to the Great Plains, western United States, *J. Geophys. Res.*, *105*, 13,715–13,734, doi:10.1029/2000JB900021.

Schellart, W., D. Stegman, and J. Freeman (2008), Global trench migration velocities and slab migration induced upper mantle volume fluxes: Constraints to find an Earth reference frame based on minimizing viscous dissipation, *Earth Sci. Rev.*, *88*, 118–144, doi:10.1016/j.earscirev.2008.01.005.

Scoppola, B., D. Boccaletti, M. Bevis, E. Carminati, and C. Doglioni (2006), The westward drift of the lithosphere: A rotational drag?, *Geol. Soc. Am. Bull.*, *118*, 199–209, doi:10.1130/B25734.1.

Sella, G. F., T. H. Dixon, and A. L. Mao (2002), REVEL: A model for Recent plate velocities from space geodesy, *J. Geophys. Res.*, *107*(B4), 2081, doi:10.1029/2000JB000033.

Silver, P. G. (1996), Seismic anisotropy beneath the continents: Probing the depths of geology, *Annu. Rev. Earth Planet. Sci.*, *24*, 385–432, doi:10.1146/annurev.earth.24.1.385.

Silver, P. G., and W. E. Holt (2002), The mantle flow field beneath western North America, *Science*, *295*, 1054–1057, doi:10.1126/science.1066878.

Simons, F. J., and R. D. van der Hilst (2003), Seismic and mechanical anisotropy and the past and present deformation of the Australian lithosphere, *Earth Planet. Sci. Lett.*, *211*, 271–286, doi:10.1016/S0012-821X(03)00198-5.

Solomon, S. C., and N. H. Sleep (1974), Some physical models for absolute plate motions, *J. Geophys. Res.*, *79*, 2557–2567, doi:10.1029/JB079i017p02557.

Solomon, S. C., N. H. Sleep, and R. M. Richardson (1975), On the forces driving plate tectonics: Inferences from absolute plate velocities and intraplate stress, *Geophys. J. Int.*, *42*, 769–801.

Somoza, R. (1998), Updated Nazca (Farallon)-South America relative motions during the last 40 My: Implications for mountain building in the central Andean region, *J. South Am. Earth Sci.*, *11*, 211–215, doi:10.1016/S0895-9811(98)00012-1.

Stefanick, M., and D. M. Jurdy (1992), Stress observations and driving force models for the South American plate, *J. Geophys. Res.*, *97*, 11,905–11,913, doi:10.1029/91JB01798.

Steinberger, B. (2000), Plumes in a convecting mantle: Models and observations for individual hotspots, *J. Geophys. Res.*, *105*, 11,127–11,152, doi:10.1029/1999JB900398.

Steinberger, B., and M. Antretter (2006), Conduit diameter and buoyant rising speed of mantle plumes: Implications for the motion of hot spots and shape of plume conduits, *Geochem. Geophys. Geosyst.*, *7*, Q11018, doi:10.1029/2006GC001409.

Steinberger, B., R. Sutherland, and R. J. O'Connell (2004), Prediction of Emperor-Hawaii seamount locations from a revised model of global plate motion and mantle flow, *Nature*, *430*, 167–173, doi:10.1038/nature02660.

Su, W., R. L. Woodward, and A. M. Dziewonski (1994), Degree 12 model of shear velocity heterogeneity in the mantle, *J. Geophys. Res.*, *99*, 6945–6980, doi:10.1029/93JB03408.

Tarduno, J. A., and J. Gee (1995), Large-scale motion between Pacific and Atlantic hotspots, *Nature*, *378*, 477–480, doi:10.1038/378477a0.

Tarduno, J. A., et al. (2003), The Emperor seamounts: Southward motion of the Hawaiian hotspot plume in Earth's mantle, *Science*, *301*, 1064–1069, doi:10.1126/science.1086442.

Tommasi, A. (1998), Forward modeling of the development of seismic anisotropy in the upper mantle, *Earth Planet. Sci. Lett.*, *160*, 1–13, doi:10.1016/S0012-821X(98)00081-8.

Tommasi, A., A. Vauchez, and R. Russo (1996), Seismic anisotropy in ocean basins: Resistive drag of the sublithospheric mantle?, *Geophys. Res. Lett.*, *23*, 2991–2994, doi:10.1029/96GL02891.

Torsvik, T. H., R. D. Müller, R. van der Voo, B. Steinberger, and C. Gaina (2008), Global plate motion frames: Toward a unified model, *Rev. Geophys.*, *46*, RG3004, doi:10.1029/2007RG000227.

Ucisik, N., Ó. Gudmundsson, W. Hanka, T. Dahl-Jensen, K. Mosegaard, and K. Priestley (2008), Variations of shear-wave splitting in Greenland: Mantle anisotropy and possible impact of the Iceland plume, *Tectonophysics*, *462*, 137–148, doi:10.1016/j.tecto.2007.11.074.

Vinnik, L. P., L. I. Makeyeva, A. Milev, and A. Y. Usenko (1992), Global patterns of azimuthal anisotropy and deformations in the continental mantle, *Geophys. J. Int.*, *111*, 433–447, doi:10.1111/j.1365-246X.1992.tb02102.x.

Waite, G. P., R. B. Smith, and R. M. Allen (2006), VP and VS structure of the Yellowstone hot spot from teleseismic tomography: Evidence for an upper mantle plume, *J. Geophys. Res.*, *111*, B04303, doi:10.1029/2005JB003867.

Walker, K. T., G. R. Bokelmann, S. L. Klemperer, and G. Bock (2005), Shear-wave splitting around the Eifel hotspot: Evidence for a mantle upwelling, *Geophys. J. Int.*, *163*, 962–980, doi:10.1111/j.1365-246X.2005.02636.x.

Wang, S., and M. Liu (2006), Moving hotspots or reorganized plates?, *Geology*, *34*, 465–468, doi:10.1130/G22236.1.

Wang, S., and R. Wang (2001), Current plate velocities relative to hotspots: Implications for hotspot motion, mantle viscosity and global reference frame, *Earth Planet. Sci. Lett.*, *189*, 133–140, doi:10.1016/S0012-821X(01)00351-X.

Wessel, P., and W. H. F. Smith (1991), Free software helps map and display data, *Eos Trans. AGU*, *72*(41), 441, doi:10.1029/90EO00319.

Wilson, J. T. (1963), A possible origin of the Hawaiian Islands, *Can. J. Phys.*, *41*, 863–868.

Wolfe, C. J., and P. G. Silver (1998), Seismic anisotropy of oceanic upper mantle: Shear wave splitting methodologies and observations, *J. Geophys. Res.*, *103*, 749–771, doi:10.1029/97JB02023.

Wolfe, C. J., and S. C. Solomon (1998), Shear-wave splitting and implications for mantle flow beneath the MELT region of the East Pacific Rise, *Science*, *280*, 1230–1232, doi:10.1126/science.280.5367.1230.

Wüllner, U., U. R. Christensen, and M. Jordan (2006), Joint geodynamical and seismic modelling of the Eifel plume, *Geophys. J. Int.*, *165*, 357–372, doi:10.1111/j.1365-246X.2006.02906.x.

Yuan, H., and K. Dueker (2005), Teleseismic *P* wave tomogram of the Yellowstone plume, *Geophys. Res. Lett.*, *32*, L07304, doi:10.1029/2004GL022056.

Yuan, H., K. Dueker, and D. L. Schutt (2008), Testing five of the simplest upper mantle anisotropic velocity parameterizations using teleseismic S and SKS data from the Billings, Montana PASSCAL array, *J. Geophys. Res.*, *113*, B03304, doi:10.1029/2007JB005092.

Zhang, S., and S. Karato (1995), Lattice preferred orientation of olivine aggregates deformed in simple shear, *Nature*, *375*, 774–777, doi:10.1038/375774a0.

Zhao, D. (2001), Seismic structure and origin of hotspots and mantle plumes, *Earth Planet. Sci. Lett.*, *192*, 251–265, doi:10.1016/S0012-821X(01)00465-4.

Zhao, D. (2007), Seismic images under 60 hotspots: Search for mantle plumes, *Gondwana Res.*, *12*, 335–355, doi:10.1016/j.gr.2007.03.001.

Zhong, S. (2001), Role of ocean-continent contrast and continental keels on plate motion, net rotation of lithosphere, and the geoid, *J. Geophys. Res.*, *106*, 703–712, doi:10.1029/2000JB900364.

C. Kreemer, Nevada Bureau of Mines and Geology, University of Nevada, Reno, 1664 North Virginia Street, Mail Stop 178, Reno, NV 89557-0088, USA. (kreemer@unr.edu)